Discovery of a cryptic site at the interface 2 of TEAD – Towards a new family of YAP/TAZ-TEAD inhibitors

Manon Sturbaut, Fabrice Bailly, Mathilde Coevoet, Pasquale Sileo, Martine Pugniere, Maxime Liberelle, Romain Magnez, Xavier Thuru, Marie-Christine Chartier-Harlin, Patricia Melnyk, et al.

DISCOVERY OF A CRYPTIC SITE AT THE INTERFACE 2 OF TEAD – TOWARDS A NEW FAMILY OF YAP/TAZ-TEAD INHIBITORS

Manon Sturbaut, [&] Fabrice Bailly, [&] Mathilde Coevoet, [&] Pasquale Sileo, [&] Martine Pugnière, [§] Maxime Liberelle, [&] Romain Magnez, [#] Xavier Thuru, [#] Marie-Christine Chartier-Harlin, [&] Patricia Melnyk, [&] Muriel Gelin, [‡] Frédéric Allemand, [‡] Jean-François Guichou, [‡*] Philippe Cotelle [&,£*]

[&] Univ Lille, INSERM, CHU Lille, UMR-S 1172, Lille Neuroscience and Cognition Research Center, F-59000, Lille, France

[§] Institut de Recherche en Cancérologie de Montpellier (IRCM) INSERM U1194 – ICM- UM 208 rue des Apothicaires, F-34298 Montpellier Cedex 5, France

[#] Univ. Lille, CNRS, Inserm, CHU Lille, IRCL, UMR9020 – UMR1277 - Canther – Cancer Heterogeneity, Plasticity and Resistance to Therapies, Platform of Integrative Chemical Biology F-59000 Lille, France

[‡] Centre de Biologie Structurale (CBS), CNRS, INSERM, Univ Montpellier, Montpellier, France

[£] ENSCL-Centrale Lille, CS 90108, F-59652 Villeneuve d'Ascq Cedex, France

* Corresponding Authors. E-mail address: guichou@cbs.cnrs.fr (Guichou, J.F.); philippe.cotelle@univ-lille.fr (Cotelle, P.)

ABSTRACT

The Hippo pathway is involved in organ size control and tissue homeostasis by regulating cell growth, proliferation and apoptosis. It controls the phosphorylation of the transcription co-activator YAP (Yes associated protein) and TAZ (Transcriptional coactivator with PDZ-binding motif) in order to control their nuclear import and their interaction with TEAD (Transcriptional Enhanced Associated Domain). YAP, TAZ and TEADs are dysregulated in several cancers making YAP/TAZ-TEAD interaction a new emerging anti-cancer target. We report the synthesis of a set of trisubstituted pyrazoles which bind to hTEAD2 at the interface 2 revealing for the first time a cryptic pocket created by the movement of the phenol ring of Y382. Compound **6** disrupts YAP/TAZ-TEAD interaction in HEK293T cells and inhibits TEAD target genes and cell proliferation in MDA-MB-231 cells. Compound **6** is therefore the first inhibitor of YAP/TAZ-TEAD targeting interface 2. This molecule could serve with other pan-TEAD inhibitors such as interface 3 ligands, for the delineation of the relative importance of VGLL *vs* YAP/TAZ in a given cellular model.

KEYWORDS

TEAD inhibition, TEAD cryptic binding pocket, interface 2, binding assays, Hippo pathway

INTRODUCTION

The Hippo pathway is involved in organ size control and tissue homeostasis by regulating cell growth, proliferation and apoptosis. It consists in a cascade of kinases including Mst1/2 (mammalian ste20-like protein kinase), Sav1 (scaffold protein Salvador), Lats1/2 (large tumor suppressor kinase) and Mob proteins (mps one binder kinase), which regulates the phosphorylation of the transcription co-activator YAP (Yes associated protein) and TAZ (Transcriptional coactivator with PDZ-binding motif) in order to control their nuclear import and their interaction with TEAD (Transcriptional Enhanced Associated Domain) [1].

The phosphorylation of S127 of YAP (S89 in TAZ) promotes its cytoplasmic retention by the protein 14-3-3 and the phosphorylation of S381 (S311 in TAZ) induces its degradation. Conversely, unphosphorylated, YAP and TAZ enter into the nucleus, interact with TEAD and drive the target gene expressions in charge of cell proliferation and apoptosis avoidance such as CTGF (connective tissue growth factor), Cyr61 (cysteine-rich angiogenic protein), Survivin (also known as Birc-5) and AXL.

In the nucleus, YAP and TAZ compete with other natural TEAD ligands, namely VGLL (Transcriptional cofactor Vestigial like protein family) which are nuclear regulators of the transcriptional activity of TEADs [2]. More recently FAM181A and FAM181B, two new TEAD interactors have been identified [3].

These proteins are expressed most prominently in neural tissues, where Fam181A is exclusively expressed during embryonic development [4].

Several stimuli such as mechanical force, cell adhesion, serum starvation, or energy stress promote activation of kinases and regulate YAP/TAZ localization. In contrast, osmotic stress, high cell density and cell detachment induce cytoplasmic translocation of TEAD [5]. A dysregulation of this equilibrium brings to abnormal and excessive proliferation leading to cancer where YAP/TAZ and TEAD are overexpressed [6]. Thus, inhibition of YAP/TAZ-TEAD complexes is a pertinent strategy for cancer therapy [7].

YAP/TAZ and TEADs form a complex through the interaction of the N-terminal domain of YAP (and TAZ) (TEAD Binding Domain: TBD) and the C-terminal domain of TEAD (YAP/TAZ Binding Domain: Y/TBD). In their pioneer work, Li *et al*. [8] (Figure 1) defined the three interfaces of contact between $TEAD1_{209-426}$ and YAP_{50-171} and their respective importance in the binding as follows: interface 3 (in red on Figure 1A) > interface 2 (in green) > interface 1 (in blue). However, the minimal fragment of YAP or TAZ which gives a nanomolar range binding constant corresponds to interfaces 2 and 3, [9] while, Kd's of $mVGLL1_{27-56}$ are in the same nanomolar range than YAP and TAZ although slightly superior while VGLL do not interact with TEAD at the interface 3 [10]. Protein fragments only composed of the Ω-loop present only micromolar affinities [3]. Whereas the YAP Ω-loop is considered to be the "hot spot" of the

YAP-TEAD interaction, it was shown that the folding of the YAP α-helix is firstly formed (interface 2) before interface 3 formation [11]. Interfaces 2 and 3 correspond to the external predicted druggable sites in green and red (Figure 1B) [12]. In 2016, was reported for the first time, that Y/TBD of TEAD2 and TEAD3 are palmitoylated in an internal hydrophobic pocket [13, 14]. This palmitoylation is required for the stability of TEAD, the interaction with YAP or TAZ and regulates the output of the Hippo pathway. This internal pocket clearly appears as the third druggable site of TEAD (in purple, Figure 1B).

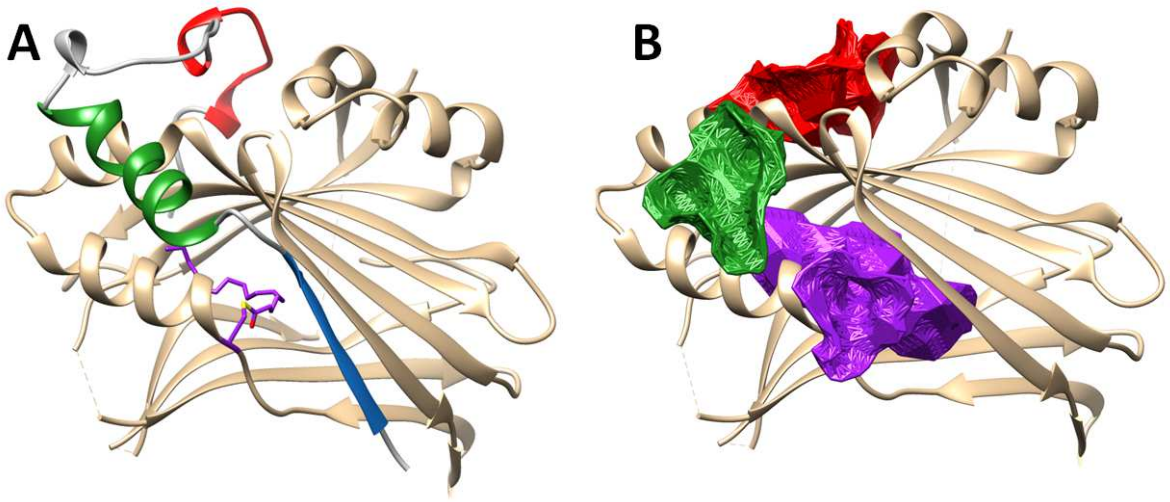

Figure 1: (A): The 3D-structure model built by superimposition of hYAP2$_{50\text{-}171}$-hTEAD1$_{209\text{-}426}$ complex (PDB code 3KYS) and hTEAD2$_{217\text{-}447}$ (PDB code 5EMV) with interface 1 (blue), 2 (green) and 3 (red); (B): The three predicted druggable sites of TEAD (interface 2 (green), interface 3 (red) and internal pocket (purple).

Chemical control of the Hippo pathway can be divided into three main strategies: (i) favor the phosphorylation [15] or the nuclear import of YAP or TAZ, (ii) physically inhibit YAP/TAZ-TEAD interaction, (iii) interfer on the YAP/TAZ-TEAD transcriptional targets.

These different strategies have been reviewed in detail by Pobbati and Hong [16].

Considering the second strategy, modified linear and cyclic YAP-like peptides and a peptide composed of the VGLL4 interface 2 domain and the YAP interface 3 domain (super-TDU) were firstly developed to compete with YAP for binding TEADs [17-19]. These modified peptides present high affinity for TEAD. Only recently, the first non-peptidic inhibitor, CPD3.1 (Figure 2), targeting the interface 3 was published [20]. As a non-selective YAP-TEAD inhibitor, CPD3.1 has an IC_{50} ranging between 33 and 44 µM on the four members of TEAD family as measured in HeLa cells transfected by a Gal4-luc reporter together with the vectors for Gal4-TEADx. Prior to the discovery of the presence of palmitate in the internal pocket of TEAD, Pobbati *et al.* [21] identified niflumic, bromoflufenamic and flufenamic acids (Figure 2), as TEAD ligands of the central pocket. While niflumic acid has a K_D of 28 µM for TEAD4 (measured by isothermal calorimetry), it only presents cellular effect at 150 µM. Bum-Erdene *et al.* [22] reported a small molecule inhibiting YAP-TEAD complex transcriptional activity through the presumed formation of a

covalent bond with the cysteine residue in the central pocket. Using fluorescence polarization experiments, the authors were able to measure the inhibitory activity of their compounds for the YAP-TEAD4 interaction. TED-347 (Figure 2) possessed an EC_{50} of 5.9 μM and a similar IC_{50} in a HEK293 cell-based assay. Not surprisingly, TEAD-347 was found to be toxic in EGFR-mutant NSCLC cell lines and replaced by another covalent TEAD ligand which bears an acrylamide moiety [23]. This new compound bearing a vinylamide moiety (MYC-01-037, (Figure 2)) is supposed to covalently bind to C359 (TEAD1) in the palmitate pocket as another vinylsulfamide (DCTEAD-02 [24]). and K-379 [25], Figure 2). But the first ligand of the palmitate pocket reported so far is MGH-CP1 (Figure 2) [26, 27] which was very recently followed by two new compounds (Compounds 1 and 2, Figure 2) developed by Genentech and Roche Pharma [28].

During the preparation of this manuscript, inhibitors of hTEAD autopalmitoylation patented by Vivace Therapeutics [29, 30] have been reported. Interestingly, VT103 (Figure 2) is the first selective inhibitor of hTEAD1 autopalmitoylation while VT107 (Figure 2) is 50 fold less active than its enantiomer [31].

A fragment based-approach allowed the identification of one hit (fragment 1, Figure 2) which binds to YAP-binding interface 2 of TEAD [32]. Its affinity for

mTEAD4 is very low (300-1400 μM) and it has a detectable cellular activity only at very high concentration (750 μM, @ 33%).

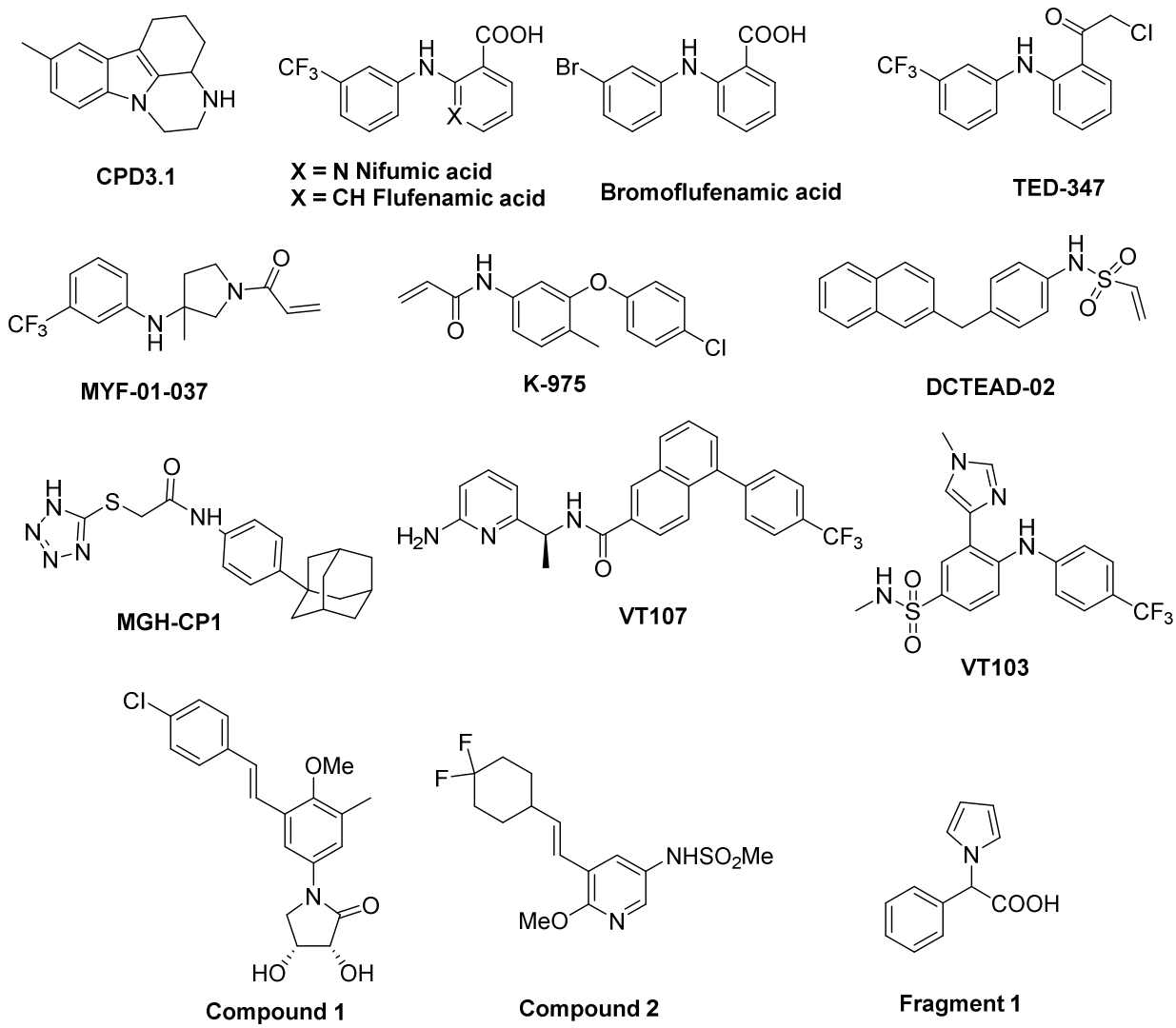

Figure 2. A set of the most important TEAD ligands reported to date

In spite of a growing research activity as attested by the number of recently published inhibitors, the design of TEAD ligands is still in its infancy with micromolar activities and only one selective TEAD1 ligand was reported to date [31].

Here, we report the first TEAD inhibitors of the interface 2 which allowed us to identify for the first time a cryptic site of TEAD C-terminal domain.

We discovered a series of trisubstituted pyrazoles (Scheme 1) which bind to hTEAD2 in an unapparent/unrevealed cryptic pocket situated at the end of one of the alpha-helix of TEAD implicated in the interface 2. The crystallographic structures of five complexes between hTEAD2 and our ligands were resolved at high resolution. Differential scanning fluorimetry (NanoDSF) experiments allowed us to define a specific profile of –dF/dT = f(T) curves. Affinity constants for hTEAD2 were measured in cell lysate by microscale thermophoresis (MST). Some of our compounds proved to be efficient in cellular assays (TEAD transcriptional activity in HEK-293T cells and TEAD target gene expression in breast cancer cell lines).

RESULTS

Synthesis of a series of TEAD ligands

We previously screened a protein-protein interface inhibitors enriched library (175000 chemical compounds) against the interface 3, using the first X-ray structure of the hYAP-hTEAD1 complex (PDB 3KYS) and identified a first hit 1 (Scheme 1) with inhibitory properties in the micromolar range (IC_{50} = 6.5 µM) in a luciferase gene reporter assay [33]. This hit 1 was optimized into hit 2 (Scheme 1) which presents an IC_{50} of 1.7 µM in the same luciferase assay [34].

To overcome solubility problems we use deconstruct strategy and decided to keep the 3,4-dichlorophenyl ring and suppress the isatin moiety and replace the central triazole ring by a diazole ring to create a small library of 3-(3,4-dichlorophenyl)-1*H*-pyrazole-4-carboxylates or carboxamides where *N*-1 was substituted by alkylamine or alkylcarboxylic acid arms (Scheme 1).

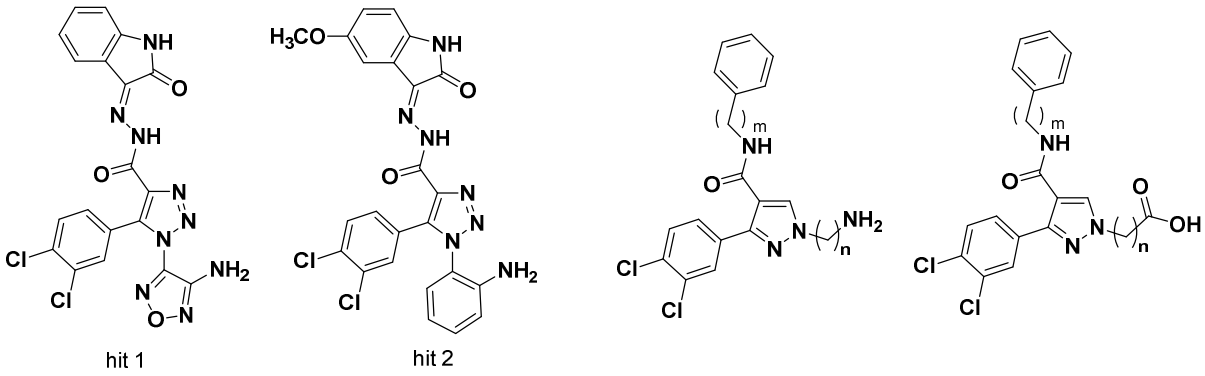

Scheme 1. Structures of previous hits leading to our new compounds

Our chemical strategy was based on the substitution of the readily available compound **1** (Scheme 2) with functionalized alkyl chains which yielded 1,3,4-trisubstituted pyrazoles as the major isomers.

Compound **1** was synthesized from ethyl 3-(3,4-dichlorophenyl)-3-oxopropanoate and *N,N*-dimethylformamide dimethylacetal according to Šenica procedure [35]. After saponification, the resulting carboxylic acid reacted with benzylamine or phenethylamine, in the presence of EDCI and HOBt to give the *N*-benzyl and *N*-phenethyl-3-(3,4-dichlorophenyl)-1*H*-pyrazole-4-carboxamide **2** and **3**, respectively. Compounds **1**-**3** were then alkylated using N-(ω-

bromoalkyl)phthalamides and the amines **4**-**12** were obtained after treatment with hydrazine hydrate. Compounds **2** and **3** were also alkylated with ethyl ω-bromopropionate or butanoate and the resulting esters were saponified to give the acids **13**-**16**.

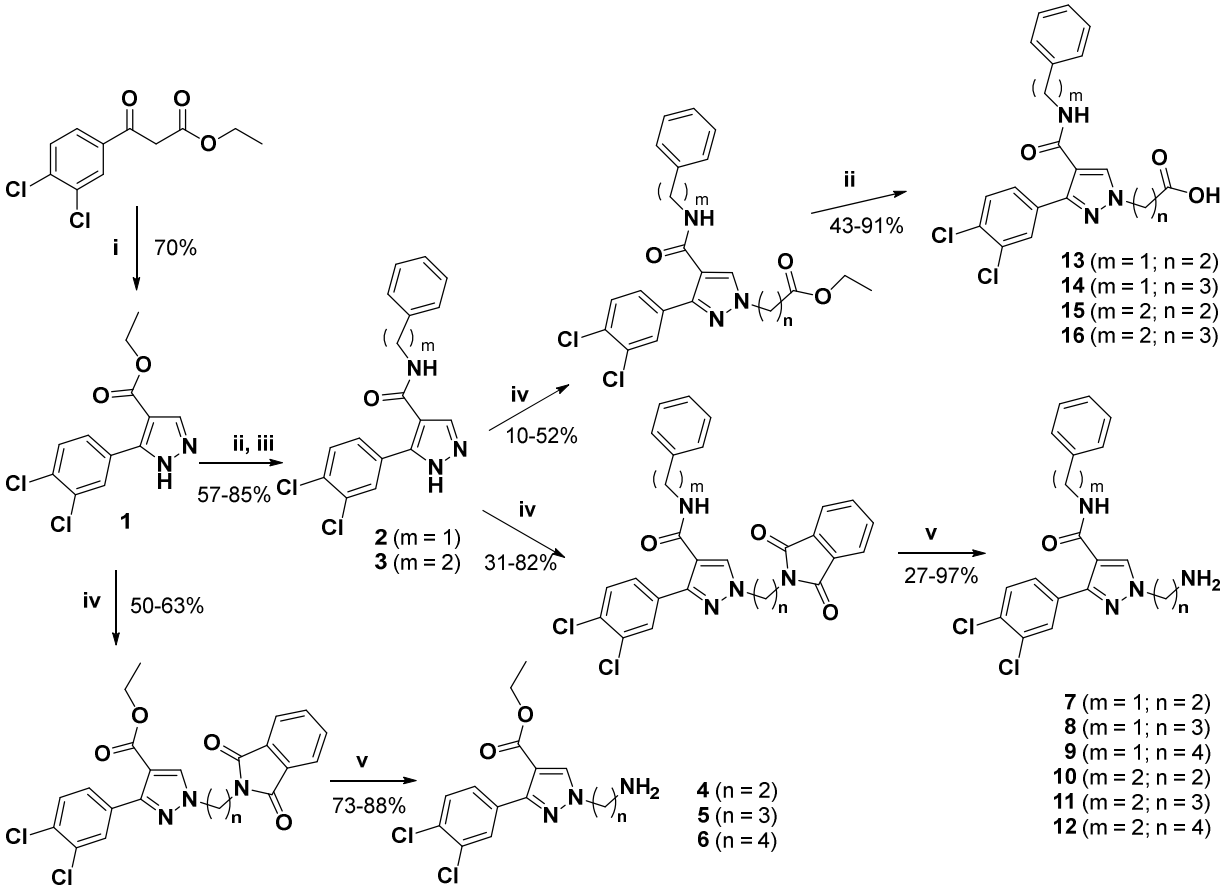

Scheme 2. i) a. DMF-DMA (1.1 eq.), toluene, reflux, 3 h; b. NH_2-NH_2.H_2O (1 eq.), EtOH, 70 °C, 5 h; ii) NaOH (10 eq.), EtOH, 78 °C, 16 h; iii) EDCI (1.2 eq.), HOBt (1.2 eq.), benzylamine or phenethylamine (1 eq.), DMF, rt, 16 h; iv) ω-Bromoalkyl esters or *N*-(ω-bromoalkyl)phthalimides (1 eq.), K_2CO_3 (2 eq.), anhydrous ACN, 82 °C, 16 h; v) NH_2-NH_2.H_2O (10 eq.), EtOH, 78 °C, 3 h.

In solution, our TEAD ligands bind to hTEAD2 at an external interface

We firstly measured the thermal stability of hTEAD2$_{217-447}$ by NanoDSF in the presence or in the absence of our compounds. NanoDSF is based on the intrinsic fluorescence of aromatic residues of the protein and avoids the possible competition of a drug with the dye used in classical TSA (Thermal Shift Assay). For hTEAD2, we observed two thermal transitions with two distinct melting temperatures (T_m) (Figure 3, red curve). According to Mesrouze *et al.* [36] the first T_m value (44.6 ± 0.5 °C) was attributed to non-acylated hTEAD2 and the second T_m value (56.8 ± 0.5 °C) to acylated hTEAD2. With a compound which binds to hTEAD2 in the palmitate pocket, we expect to observe only one T_m. Conversely with a compound which binds to hTEAD2 at an external interface, we expect to observe two new shifted T_m values. In our hand, niflumic acid (Figure 3, cyan curve) gave an intermediate T_m value of 50.3 °C. Moreover, Tang *et al.* [31] found the same tendency with their recombinant TEAD proteins with all their TEAD ligands (which bind to the internal pocket). In the presence of our compounds, the thermal stability of the protein was changed and negative or positive thermal shifts were observed for each peak of the first derived curve (-dF/dT = f(T)). The profiles of the curves are characteristic of those of TEAD-ligands which bind to TEAD on the external surface of the protein.

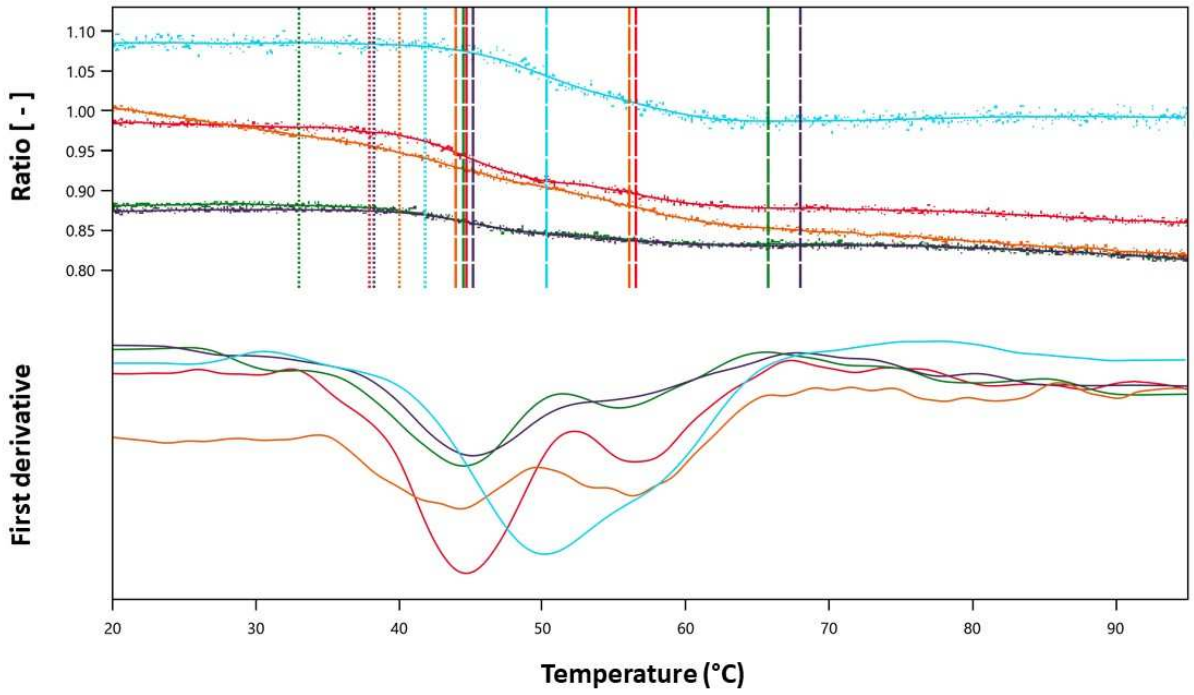

Figure 3. Representative thermograms obtained by NanoDSF for hTEAD2$_{217\text{-}447}$ protein (5 μM) in the absence (red) or in the presence of tested compounds **6** (orange), **7** (green), **14** (violet) and niflumic acid (light blue). The melting temperatures (T_m) were obtained by plotting the first derivative of the fluorescence emission (F) as a function of the temperature (–dF/dT). The curve minimum corresponds to T_m.

Acidic ligands have a better affinity towards hTEAD2 than basic ligands

The biological matrix is known to influence the affinity of a drug for its target. For example, Wienken *et al.* [37] measured a 400-fold reduction for the affinity of quercetin for its kinase PKA in human serum *vs* in buffer. In order to reflect more accurately the affinity of our drugs for hTEAD2 in complex medium, the interactions between our compounds and hTEAD2 were quantitatively measured

using microscale thermophoresis (MST) on GFP-labeled hTEAD2$_{217–447}$ in CHO-K1 cell lysate [35]. hYAP$_{50–102}$, which is the fragment which interacts with hTEAD in interfaces 2 and 3 was used as a control for MST experiments.

The affinity of hYAP$_{50–102}$ for GFP-labeled hTEAD2$_{217–447}$ is evaluated through the K_d value (96 nM) which is in accordance with the literature [38]. We measured the affinity of the compounds **6-7** and **13-15**. **7** and **13** were found to produce residual fluorescence and we were unable to properly measure their K_d values. However, **14** and **15** presented a micromolar affinity with K_d of 4.6 and 5.1 µM respectively while **6** had a lower affinity than **14** or **15** for hTEAD2 (K_d = 35 µM) (Figure 4, and Supplement figures 1, 2 and 3).

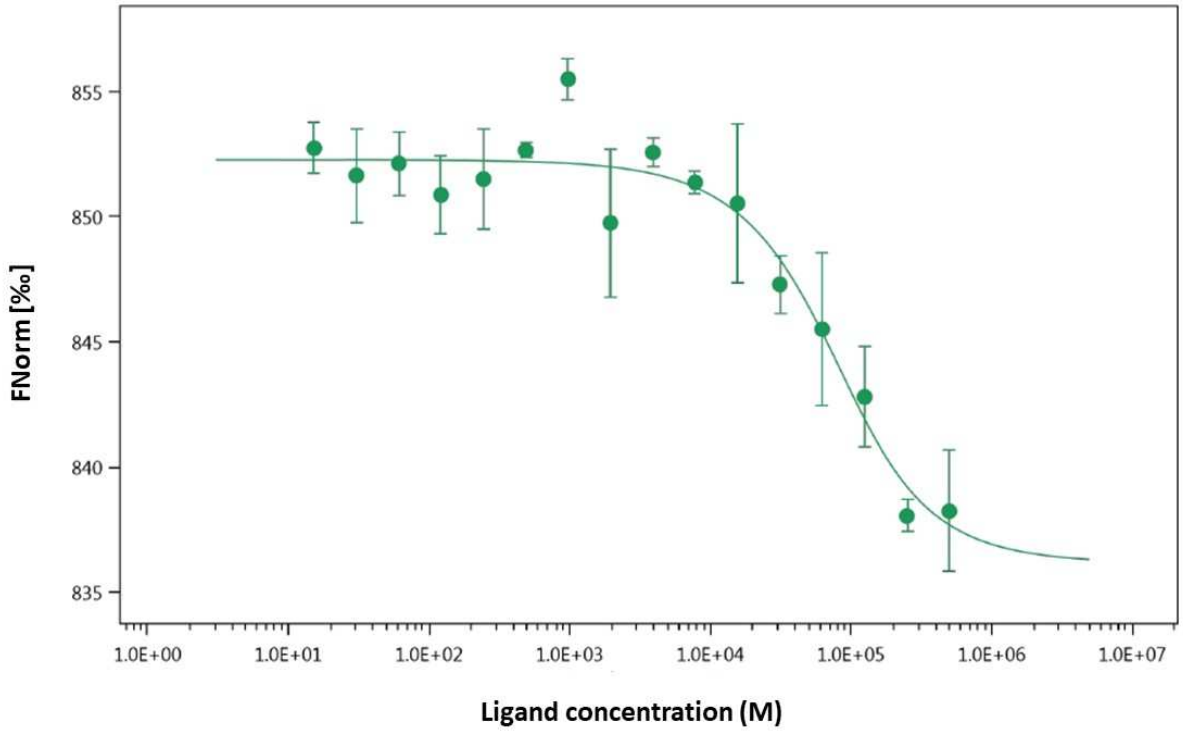

Figure 4. Titration of eGFP-hTEAD2$_{217–447}$ (30 nM) by compound **6** in CHO-K1 cell lysate; LED intensity: 100%; MST power: 40%. All the experiments have been made in triplicate on three independent cell cultures (mean ± SD, n = 3).

Our TEAD ligands bind to TEAD at a cryptic pocket situated in the interface 2

hTEAD2$_{217-447}$ crystals were soaked with compounds **4-16**. Five complexes (compounds **6**, **7**, **13**, **14** and **15**) were obtained with resolutions ranging from 2.00 to 2.22 Å (Figure 5A, Supplement Tables 1 and 2 and Supplement Figures 4-8). The structures were solved in space group C2 with two TEAD per asymmetric unit. In all the internal pocket of the TEAD units, a myristate/palmitate molecule is present either free, or bonded to the sulfur atom of C380 (thioester) or to the nitrogen atom of K357 (amide) as previously reported [8, 14, 22]. hTEAD2 crystallized as a dimer in the asymmetric unit cell, all the complexes were obtained with only one compound because the second cryptic pocket is not accessible due to the crystal packing. The five compounds fitted hTEAD2 in a very similar manner at the larger end of the binding groove formed by hTEAD2 α3 and α4 helices (residues 381-405) involved in the interface 2 with YAP α1 helix (residues 61-73) (Figure 5A).

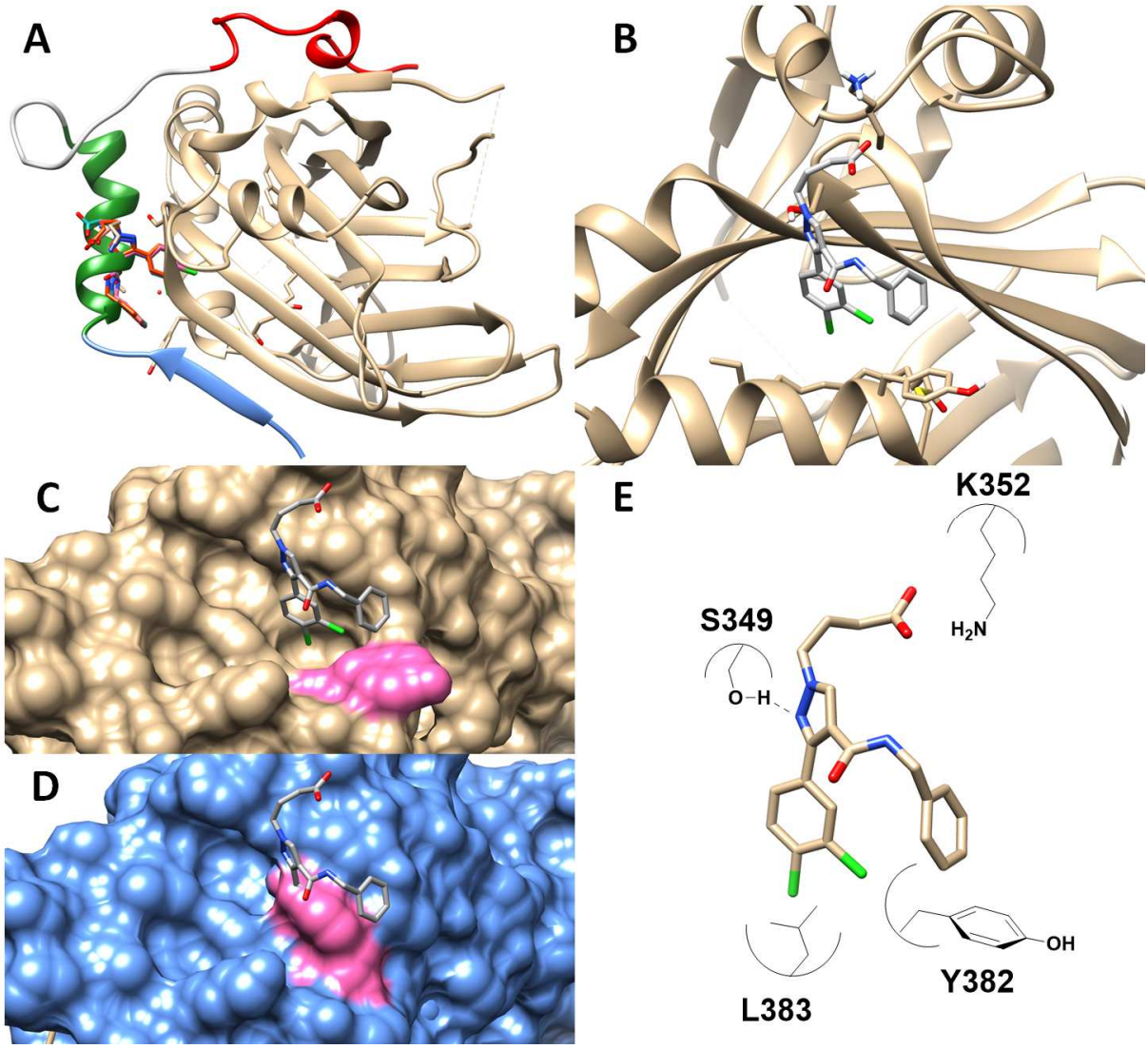

Figure 5. (A) Superimposition of the crystal structure of hTEAD2$_{217-447}$ in complex with compounds **6**, **7**, **13**, **14** and **15** (PDB codes: 6S6J, 6S66, 6S64, 6S60 and 5S69, respectively) and of hTEAD1$_{210-426}$ in complex with hYAP$_{50-100}$ (PDB code: 3KYS); (B) Zooming on the compound **14** environment; (C) and (D) The cryptic pocket: zooming on the pocket created (PDB code: 6S60) (in tan) and superimposition of compound **14** on hTEAD2$_{217-447}$ (PDB code: 5 EMV) (in blue, Y382 is in pink); (E) Principal interactions of compound **14** with hTEAD2.

A cryptic pocket (Figure 5C and 5D) is created where the 3,4-dichlorophenyl moiety is perfectly inserted in. This new pocket is due to the flipping of Y382 side chain. The ligand's position is at the amide bond between L65 and D64 residues of YAP. The unsubstituted nitrogen of the pyrazole is engaged in a hydrogen bond with the alcohol function of S349 of TEAD2 and therefore replaces the hydrogen bond made by the carboxylate function of D64 of YAP and the alcohol function of S349. The phenyl ring of compounds **7** and **13-15** does an angle of about 80 ° with the phenol ring of Y382 and the acidic function of compounds **13-15** is oriented towards the terminal ammonium of K352 (Figure 5B and 5E) but without making any hydrogen bond with this residue. The bottom of the cryptic pocket consists in the isobutyl group of L383 which is specific of hTEAD2 (other TEADs have a methionine residue at this position (M362 for TEAD1, M371 for TEAD3 and M370 for TEAD4). Analysis of other crystal structures of hTEAD2 (5EMV for example) and other hTEADs showed the cryptic pocket pre-exists and is masked by Y382. The shape does not significantly differ amongst the different TEADs.

*Compound **6** inhibits TEAD-dependent target gene expression*

We firstly measured the TEAD transcriptional activity in transfected HEK293T cells in the presence of our compounds (**5-9** and **11-16**, 10 µM, 16 h) using a

previously used TEAD reporter luciferase assay [33]. We used Dasatinib [39] at a concentration of 100 nM and MGH-CP1, a patented compound that was reported to bind to TEAD in the palmitate pocket, at a concentration of 10 µM [27], as references. We measured the β-galactosidase activity in order to normalize the luciferase activities and to qualitatively estimate the cytotoxicity of the tested compounds. In case of significant decrease of β-galactosidase signal after 24 h post transfection, the luciferase activity result was not retained. The cell viability was visually controlled after treatment. The reporter activities are given on Figure 6. Compounds **4** and **10** were found to be too instable to be tested in cells. In our series, we found that all the amides with a ω-aminoalkyl chain (**7-12**) presented a dramatic decrease in β-galactosidase activity which reflects an intrinsic toxicity and the amides with a ω-carboxyalkyl chain (**13-16**) were almost inactive in spite of a good affinity for **14** and **15** measured by MST. Finally, aminoesters (**5-6**) were found to be the most active compounds of the series. The affinity was measured on eGFP-TEAD2 in lysate whereas the TEAD transcriptional activity was measure in cells, the differences between **6** and **14-15** may be due to a lower nucleus penetration for the acidic **14**-**15** than for the basic **6**.

Dose-response curves for compound **6** gave an IC_{50} of 4.5 ± 1.5 µM (Supplement Figure 9). Here again, we found some discrepancies between the affinity for eGPF-TEAD2 and the inhibition of TEAD transcriptional activity which could be attributed to differences between the method and the target. By

MST we used hTEAD2$_{217-447}$ while HEK293T cells expressed TEAD2 at very low levels [31]. We measured the effects of compound **6** (10 µM) and Dasatinib (100 nM) on the RNA and expression of AXL, CTGF and Cyr61 and protein expression of AXL, CTGF, Cyr61, and Survivin (Birc-5) (Supplement Figure 10) in MDA-MB231 cells. Similar effects were also found in HeLa cell lines (Supplement Figure 11) but not on SH-SY5Y cell lines which do not express YAP or TAZ (data not shown). The results are reported on Figure 7. In good correlation with the reporter assay, compound **6** inhibited the expression of the four target proteins. The same tendency was found with the RNA expression of AXL, CTGF and Cyr61 after only 24h of treatment.

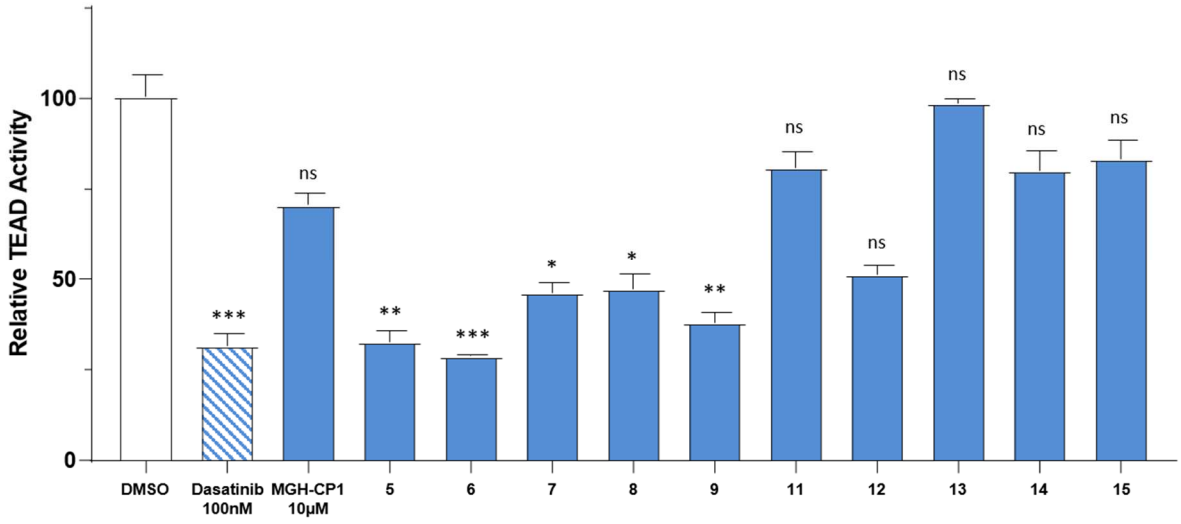

Figure 6. TEAD reporter luciferase activity observed in HEK293T cells treated with compounds **5-9** and **11-16** (10 µM), MGH-CP1, or dasatinib after 16 h post transfection. Data are representative of at least three independent experiments in tri biological replicates; mean ± SD, n = 3. p values were calculated using

Kruskal-Wallis tests. ns = not significant, * = $p < 0.05$, ** = $p < 0.01$, *** = $p < 0.001$

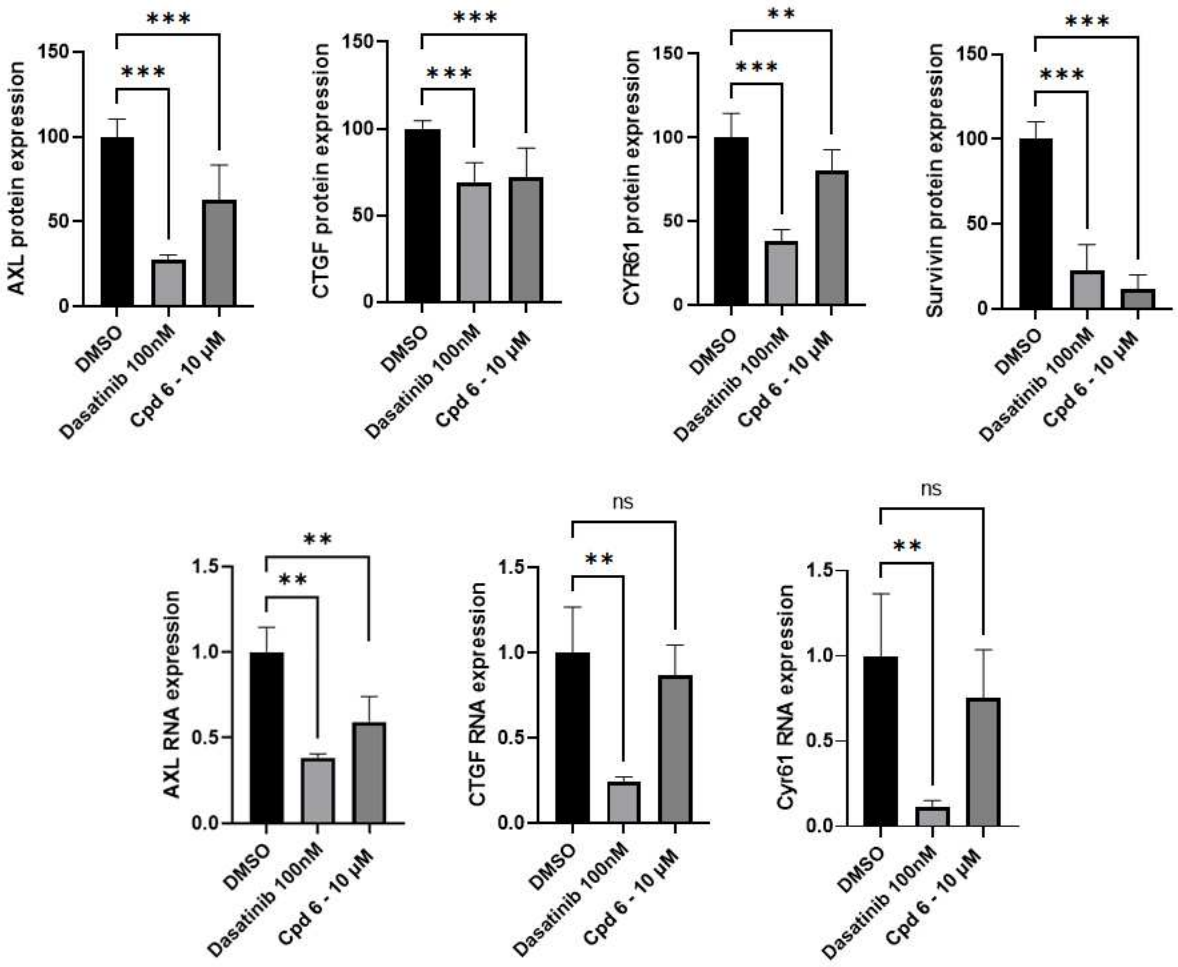

Figure 7. Effects of Dasanitib and compound **6** on protein production of AXL, CTGF, Cyr61, and Survivin in MDA-MB-231 cells after 48h exposure and RNA expression of AXL, CTGF and Cyr61 in MDA-MB-231 cells after 24h exposure. Data are representative of at least three independent experiments in tri biological replicates; mean ± SD, n = 3. p values were calculated using Kruskal-Wallis tests.

ns = not significant, * = $p < 0.05$, ** = $p < 0.01$, *** = $p < 0.001$

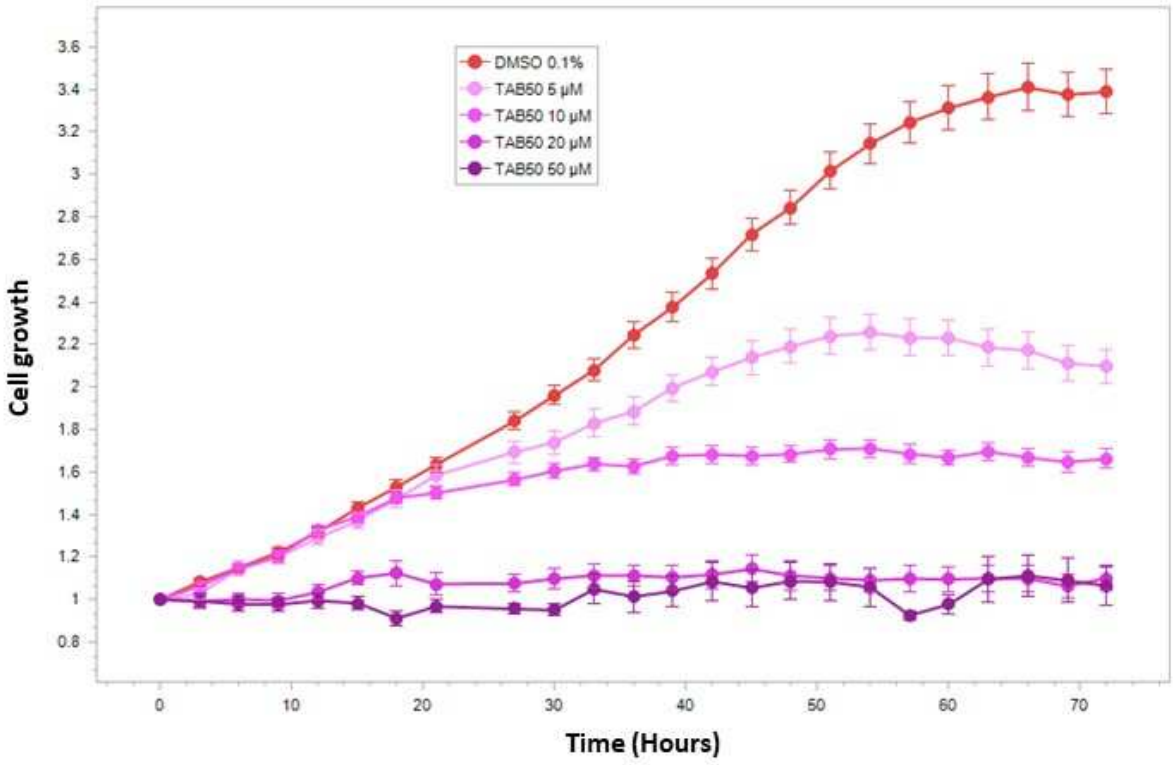

Figure 8. Effect of compound **6** on the kinetic cell growth of MDA-MB-231 cells at low confluence (0.25 x 10^4 cells/well) (mean ± SD, n = 3).

Finally, we measured the effect of compound **6** on the proliferation of MDA-MB-231 cells at low confluence. Cells were plated at low confluence and exposed to compound **6** at different concentrations. Images were made every 3 h

until control DMSO-treated cells reached a plateau. Compound **6** decreased the cell proliferation by 40 % at 5 µM and by 60 % at 10 µM after 48 h (Figure 8).

DISCUSSION AND CONCLUSION

We herein report the discovery of the first inhibitors of the YAP/TAZ-TEAD interactions targeting the interface 2. The structures of five complexes with a high resolution allowed us to discover and characterize for the first time a cryptic site on the common surface of the YAP/TAZ/VGLL-binding domain of TEAD [40, 41]. The phenol moiety of Y382, which, generally points towards the interface 2 (in the direction of S349) groove in almost all previous crystal structures of TEAD2, moved away. Re-analysis of all the TEAD units found in published crystallographic structures showed that, in two monomers (A and C) of mTEAD4 of the crystal complex of TAZ-mTEAD4 (PDB code: 5 GNO), this tyrosine residue (Y362 (Y382 in hTEAD2)) pointed towards C360 making a hydrogen bond with the thiol hydrogen atom when C360 is not covalently bonded to palmitate and in the two other monomers (B and D) pointed towards S329 (S349 in hTEAD2) (Figure 9). It would be of interest in the future to evaluate if Y382 plays a role in the palmitoylation of TEAD.

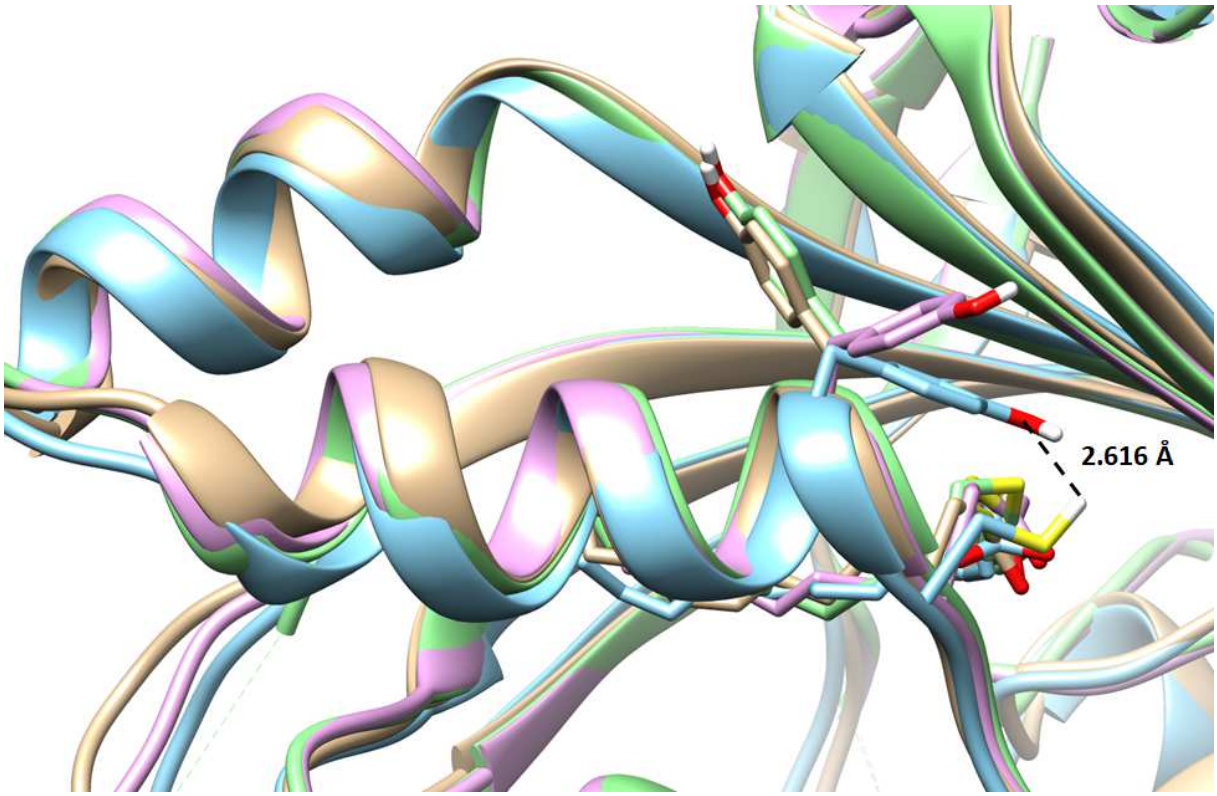

Figure 9. Superimposition of the crystal structure of hTEAD2$_{217-447}$ in complex with compound **6** (PDB codes: 6S6J, in violet), of hTEAD2$_{217-447}$ (PDB code: 5 EMV) (in green) and of mTEAD4$_{210-427}$ in complex with hTAZ$_{24-57}$ (PDB code: 5GN0, unit D in tan, unit C in blue)

The deep pocket created is occupied by the 3,4-dichlorophenyl ring of our compounds. The free nitrogen of the central pyrazole of our drugs replaced the phenolic group of Y382 and created a hydrogen bond with the hydroxyl group of S349. This residue is also involved in a specific hydrogen bond with the imidazole ring of H44 of mVGLL1 [39] or with the carboxylate function of D64 of hYAP [42]. We placed at position 4 an ethyl ester, a benzylamide or a phenethylamide group and at position 1 a ω-aminoalkyl or ω-carboxyalkyl

chain. All these variations we introduced were found in the compounds engaged in a complex with TEAD2 suggesting that the main structural element of this new class of TEAD ligand is the 3-(3,4-dichlorophenyl)-1-substituted pyrazole-4-carboxylate or carboxamide moiety. The ω-aminoalkyl or ω-carboxyalkyl arm is supposed to help N-2 to engage hydrogen bond with the hydroxyl group of S349 through its electro-donating effect and head away the interface 2. We previously demonstrated the importance of the 3,4-dichlorophenyl moiety [34] and we planned in the future to delineate the relative importance of each chlorine atom of this moiety.

Kaan *et al.* [32] have previously reported the discovery of a fragment that targets the mTEAD4 interface 2 (pdb code: 5XJD). This fragment symmetrically binds to two molecules of TEAD. It is located closely to K389 at the third loop of α3 helix while our compounds bind to a pocket created by the flipping of Y382 (first loop of α3 helix) (Supplement Figure 12). Computational ligand-mapping study allowed Kaan *et al.* to identify putative cryptic binding sites in mTEAD4. However, it is difficult for us to know their exact positions and if this study predicted our cryptic pocket.

As clearly shown before, expression of TEADs by *Escherichia coli* afforded a mixture of acylated and non-acylated TEADs. A ligand which binds to the palmitate pocket of TEAD gives rise to only one thermal transition while a ligand which binds to the external surface of TEAD affords two thermal transitions. NanoDSF allowed us to observe two thermal transitions with distinct

melting temperatures and confirm our compounds bind externally to TEAD YBD.

Affinity constants for e-GFP-TEAD2 in cell lysate were measured for three of the five compounds which afforded crystal structures. Measured affinity are in the micromolar range.

Compound **6** inhibits TEAD-dependent transcriptional activity in HEK293T cells transfected with the reporter construct (8xGTIIC-Luciferase) with an IC_{50} of 4.5 µM which is comparable to its capability to induce a 50 % inhibition of proliferation of MDA-MB-231 cells at 5 µM at the same level than in MDA-MB-231 cells. Compound **6** effectively inhibits expression of proliferation, survival and anti-apoptotic YAP-TEAD target genes (Cyr61, CTGF, AXL and Survivin) at protein and mRNA levels in the same cell line.

These molecules could serve with other pan-TEAD inhibitors such as CPD3.1 [20] which is considered to target interface 3, for the delineation of the relative importance of VGLL *vs* YAP/TAZ in a given cellular model. VGLLs are known to be antagonists of YAP/TAZ-TEAD complexes but may be tumor suppressor [43, 44] or associated with a poor prognostic [45-48]. For example, VGLL4 is a tumor suppressor in lung, gastric and colorectal cancers but high VGLL4 correlates with poor clinical outcomes in non-small-cell lung cancer [49]. Compound **6** represents a solid structural basis to be optimized for the development of new therapies for the treatment of cancer particularly where YAP or TAZ are overexpressed [6].

During the preparation of this article, was reported the design and characterization of a stabilized protein tertiary structure that acts as an inhibitor of the interaction between the transcription factor TEAD and its co-repressor VGLL4 [50]. This eicosapeptide linked to Tat sequence through a PEG2 linker presents a crosslink between the acid function of a glutamic residue and the ammonium function of a lysine residue. It binds to mTEAD4 as our compounds in the interface 2 but was found higher inhibitor of VGLL4 than YAP and therefore activates YAP-TEAD interaction, increases mRNA target genes levels in cardiomyocytes and accelerates wound healing of RKO cells. Superimposition of the crystal structures (6SBA and 6S60) showed our molecules only overlap at the end of interface 2 with one end of one of the helix of the eicosapeptide (Supplement figure 13).

EXPERIMENTAL SECTION

Chemistry. General details. All reagents and solvents were purchased from Aldrich-Chimie (Saint-Quentin-Fallavier, France) of ACS reagent grade and were used as provided. All reagents and solvents were purchased and used without further purification. Reactions were monitored by TLC performed on Macherey Nagel Alugram® Sil 60/UV254 sheets (thickness 0.2 mm). Some purification of products was carried out by flash column chromatography (FC) using Macherey Nagel silica gel (230-400 mesh). Melting points were determined on a BÜCHI B-540 apparatus and are uncorrected. NMR spectra

were recorded on a Bruker Avance 300 spectrometer operating at 300 MHz (^{1}H) or 75 MHz (^{13}C). Chemical shifts are in parts per million (ppm) and were referenced to the residual proton peaks in deuterated solvents. Chemical shifts are reported in δ units (ppm) and are assigned as singlets (s), doublets (d), doublets of doublets (dd), triplets (t), quartets (q), quintets (quin), sextuplets (sext), multiplets (m), and broad signals (br). Mass spectra were recorded with an LCMS (Waters Alliance Micromass ZQ 2000). LCMS analysis was performed using a Waters XBridge C18 column (5 µm particle size column, dimensions 50 mm x 4.6 mm). Reported *m/z* correspond to the most abundant isotope (^{35}Cl in the case of chlorine). A gradient starting from 98 % H_2O/formate buffer 5 mM (pH 3.8) and reaching 100 % CH_3CN/ formate buffer 5 mM (pH 3.8) within 4 min at a flow rate of 2 mL/min was used followed by a return to the starting conditions within 1 min. Purity of final tested compounds (**5-9** and **11-16**) was > 95 % (except for **14**, purity > 94 %) as determined by high pressure liquid chromatography (HPLC) column: C18 Interchrom UPTISPHERE. Analytical HPLC was performed on a Shimadzu LC-2010AHT system equipped with a UV detector set at 254 nm and 215 nm. Compounds were dissolved in 50 mL acetonitrile and 950 mL buffer B, and injected into the system. The following eluent systems were used: buffer A (H_2O/TFA, 100:0.1) and buffer B (CH_3CN/H_2O/TFA, 80:20:0.1). HPLC retention times (HPLC t_R) were obtained at a flow rate of 0.2 mL/min for 35 min using the following conditions: a gradient run from 100 % of buffer A over 1 min, then to 100 % of

buffer B over the next 30 min. Purity of final compounds was > 95 % as determined by HPLC (see Supporting Information).

Ethyl 5-(3,4-dichlorophenyl)-1*H*-pyrazole-4-carboxylate (1). A stirred solution of ethyl 3-(3,4-dichlorophenyl)-3-oxopropanoate (2.00 g, 7.66 mmol) and *N,N*-dimethylformamide dimethyl acetal (1.00 g, 8.43 mmol) was heated at 90 °C for 3 h. After evaporation of the excess of *N,N*-dimethylformamide dimethyl acetal under reduced pressure, the crude enaminone was dissolved in EtOH (14 mL) with hydrazine monohydrate (0.38 g, 7.66 mmol) and heated at 70 °C for 2 h. After concentration under vacuum, the residue was taken up in EtOAc, washed with water. The organic phase was dried over $MgSO_4$ and concentrated under vacuum. The residue was purified by FC (DCM/MeOH 98/2) to afford **1** (1.50 g, 69 %) as a white solid (Mp = 136-138 °C). ^{1}H NMR (300 MHz, $CDCl_3$): δ 1.32 (t, 3 H, ^3J = 7.1 Hz), 4.30 (q, 2 H, ^3J = 7.1 Hz), 7.51 (d, 1 H, ^3J = 8.0 Hz); 7.63 (dd, 1 H, ^3J = 8.4 Hz, ^4J = 2.0 Hz), 7.89 (d, 1 H, ^4J = 2.0 Hz), 8.17 (s, 1 H). ^{13}C NMR (75 MHz, $CDCl_3$): δ 14.2 (CH_3), 60.6 (CH_2), 111.9 (C_{IV}), 128.5 (CH), 130.0 (CH), 131.0 (CH), 131.9 (C_{IV}), 132.4 (C_{IV}), 132.5 (C_{IV}), 137.7 (CH), 148.3 (C_{IV}), 168.9 (CO). LC-MS (ESI): *m/z* Calculated: 284.01, Found: 285.10, $[M+H]^+$, 283.10, $[M-H]^-$, t_R = 2.9 min.

***N*-Benzyl-5-(3,4-dichlorophenyl)-1*H*-pyrazole-4-carboxamide (2).** A mixture of ethyl 5-(3,4-dichlorophenyl)-1*H*-pyrazole-4-carboxylate (2.30 g, 8.07 mmol) and NaOH (3.20 g, 80.70 mmol) in ethanol (90 mL) was stirred at reflux for 16 h. After concentration under vacuum, the residue was taken up in water and

extracted with DCM. The aqueous layer was acidified with aq. 1.0 M HCl solution and extracted with EtOAc. The organic layer was dried over $MgSO_4$, concentrated under vacuum and used without purification in the next step.

5-(3,4-Dichlorophenyl)-1*H*-pyrazole-4-carboxylic acid (1.00 g, 3.89 mmol), EDCI (0.72 g, 4.67 mmol) and HOBt (0.63 g, 4.67 mmol) were dissolved in DMF (100 mL). After cooling to 5 °C, benzylamine (1 eq., 0.42 g, 0.42 mL, 3.89 mmol) was added to the mixture and the solution was stirred overnight at room temperature. After concentration under vacuum, the residue was taken up in EtOAc and washed with water. The organic layer was dried over $MgSO_4$, concentrated under vacuum and purified by FC with cyclohexane/EtOAc (10:0 → 50:50, v/v) to afford **2** (0.77 g, 57 %) as an orange powder (Mp = 174-176 °C). ^{1}H NMR (300 MHz, DMSO-*d*$_6$): δ 4.40 (d, 2 H, ^3J = 5.8 Hz), 7.30 (m, 5 H), 7.61 (d, 1 H, ^3J = 8.4 Hz), 7.70 (s, 1 H), 7.80 (dd, 1 H, ^3J = 8.4 Hz, ^4J = 1.8 Hz), 8.09 (d, 1 H, ^4J = 1.8 Hz), 8.29 (d, 1 H, ^3J = 1.1 Hz), 8.65 (t, 1 H, ^3J = 5.8 Hz). ^{13}C NMR (75 MHz, DMSO-*d*$_6$): δ 42.7 (CH_2), 115.3 (C_{IV}), 127.2 (CH), 127.7 (2 CH), 128.7 (2 CH), 128.9 (CH), 130.4 (CH), 130.5 (CH), 130.9 (2 C_{IV}), 132.0 (CH), 134.5 (C_{IV}), 140.1 (C_{IV}), 147.8 (C_{IV}), 163.5 (CO). LC-MS (ESI): *m/z* Calculated: 345.05, Found: 346.10, $[M+H]^+$, 344.20, $[M-H]^-$, t_R = 2.7 min.

5-(3,4-Dichlorophenyl)-*N*-phenethyl-1*H*-pyrazole-4-carboxamide (3). 5-(3,4-dichlorophenyl)-1*H*-pyrazole-4-carboxylic acid (1 eq., 1.30 g, 5.05 mmol), EDCI (1.2 eq., 0.94 g, 6.07 mmol) and HOBt (1.2 eq., 0.92 g, 6.07 mmol) were dissolved in DMF (125 mL). After cooling to 5 °C, phenethylamine (1 eq., 0.61

g, 0.64 mL, 5.05 mmol) was added and the mixture and was stirred overnight. After concentration under vacuum, the residue was taken up in EtOAc and washed with water. The organic layer was dried over $MgSO_4$, concentrated under vacuum and purified by FC with cyclohexane/EtOAc (10:0 → 50:50, v/v) to afford **3** (1.54 g, 85 %), as yellow solid (Mp = 201-202 °C). ^{1}H NMR (300 MHz, DMSO-d_6): δ 2.82 (t, 2 H, ^3J = 7.4 Hz), 3.44 (t, 2 H, ^3J = 7.4 Hz), 7.20-7.32 (m, 5 H), 7.62 (d, 1 H, ^3J = 8.4 Hz), 7.78 (d, 1 H, ^4J = 1.2 Hz), 8.10 (s, 1 H) 8.20 (dd, 1 H), 13.34 (brs, 1H). ^{13}C NMR (75 MHz, DMSO-d_6): δ 36.05 (CH_2), 41.2 (CH_2), 116.0 (C_{IV}), 126.9 (CH), 129.1 (C_{IV}), 129.3 (C_{IV}), 129.5 (CH), 130.8 (2 CH), 130.9 (C_{IV}), 130.9 (2 CH), 130.9 (C_{IV}), 132.2 (CH), 134.9 (CH), 140.3 (CH), 148.0 (C_{IV}), 165.9 (CO); LC-MS (ESI): *m/z* Calculated: 359.09, Found: 360.16, $[M+H]^+$, 358.27, $[M-H]^+$, t_R = 2.8 min.

General procedure for the synthesis of ethyl 1-(ω-aminoalkyl)-3-(3,4-dichlorophenyl)-1*H*-pyrazole-4-carboxylates or 1-(ω-aminoalkyl)-*N*-benzyl-3-(3,4-dichlorophenyl)-1*H*-pyrazole-4-carboxamides. A solution of *N*-benzyl-5-(3,4-dichlorophenyl)-1*H*-pyrazole-4-carboxamide (1 eq., 0.30 g, 0.87 mmol), K_2CO_3 (2 eq., 0.24 g, 1.73 mmol) and the convenient N-(ω-bromoalkyl)phthalimide (1 eq., 0.87 mmol) in anhydrous acetonitrile (15 mL) and under a nitrogen atmosphere was stirred at reflux overnight and concentrated under reduced pressure. The residue was taken up in EtOAc and washed with water. The organic layer was dried over $MgSO_4$, concentrated under vacuum and purified by FC (DCM/MeOH 98/2).

Hydrazine monohydrate (10 eq., 0.33 g, 0.32 mL, 6.71 mmol) and N-benzyl or phenethyl-5-(3,4-dichlorophenyl)-1-[2-(1,3-dioxo-2,3,3a,7a-tetrahydro-1H-isoindol-2-yl)ethyl]-1H-pyrazole-4-carboxamide (1 eq., 0.67 mmol) were dissolved in EtOH (6 mL). The mixture was stirred at reflux for 3 h then concentrated under reduced pressure, taken up in EtOAc and washed with water. The organic layer was dried over $MgSO_4$, concentrated under vacuum and purified by FC (DCM/MeOH 9/1) to afford the desired alkyl amine **4-12**.

Ethyl 1-(2-aminoethyl)-3-(3,4-dichlorophenyl)-1*H*-pyrazole-4-carboxylate (4). Following the general procedure, the compound **4** was isolated by FC (108 mg, 88 %); ^{1}H NMR (300 MHz, $CDCl_3$): δ 1.31 (t, 3 H, ^3J = 7.1 Hz), 3.26 (m, 2 H), 4.26 (m, 4 H), 7.47 (d, 1 H, ^3J = 8.4 Hz), 7.70 (dd, 1H, ^3J = 8.4 Hz, ^4J = 2.0 Hz), 7.95 (d, 1 H, ^4J = 2.0 Hz), 8.07 (s, 1 H). ^{13}C NMR (75 MHz, $CDCl_3$): δ 14.3 (CH_3), 41.6 (CH_2), 55.5 (CH_2), 60.4 (CH_2), 111.9 (C_{IV}), 128.6 (CH), 129.8 (CH), 131.1 (CH), 131.9 (C_{IV}), 132.4 (C_{IV}), 132.5 (C_{IV}), 136.0 (CH), 150.9 (C_{IV}), 162.8 (CO). LC-MS (ESI): *m/z* Calculated: 327.05, Found: 328.10, $[M+H]^+$, t_R = 2.4 min.

Ethyl 1-(2-aminopropyl)-3-(3,4-dichlorophenyl)-1*H*-pyrazole-4-carboxylate (5). Following the general procedure, the compound **5** was isolated by FC (107 mg, 83 %); ^{1}H NMR (300 MHz, DMSO-d_6): δ 1.23 (t, 3 H, ^3J = 7.1 Hz), 2.14 (quint, 2 H, ^3J = 6.9 Hz), 2.77 (t, 2 H, ^3J = 7.0 Hz), 4.19 (q, ^3J = 7.2 Hz, 2 H), 4.32 (t, 2 H, ^3J = 6.9 Hz), 7.68 (d, 1 H, ^3J = 8.4 Hz), 7.76 (dd, 1 H, ^3J = 8.4 Hz, ^4J = 1.8 Hz), 8.03 (d, 1 H, ^4J = 1.8 Hz), 8.10 (brs, 3 H) 8.52 (s, 1 H). ^{13}C NMR

(75 MHz, DMSO-d_6): δ 14.6 (CH_3), 27.9 (CH_2), 36.6 (CH_2), 49.3 (CH_2), 60.4 (CH_2), 111.2 (C_{IV}), 129.5 (CH), 130.6 (CH), 131.01 (CH), 131.04 (C_{IV}), 131.4 (C_{IV}), 133.3 (C_{IV}), 137.4 (CH), 149.5 (C_{IV}), 162.7 (CO). LC-MS (ESI): *m/z* Calculated: 341.07, Found: 342.10, $[M+H]^+$, t_R = 2.5 min.

Ethyl 1-(4-aminobutyl)-3-(3,4-dichlorophenyl)-1H-pyrazole-4-carboxylate (6). Following the general procedure, the compound **6** was isolated by FC (196 mg, 73 %); ^{1}H NMR (300 MHz, DMSO-d_6): δ 1.23 (t, 3 H, ^3J = 7.2 Hz), 1.56 (quint, 2 H, ^3J = 6.9 Hz), 1.86 (quint, 2 H, ^3J = 6.9 Hz), 2.79 (t, 2 H, ^3J = 7.2 Hz), 4.20 (t, ^3J = 7.0 Hz, 2 H), 4.22 (q, ^3J = 7.2 Hz, 2 H), 7.67 (d, 1 H, ^3J = 8.4 Hz), 7.76 (dd, 1 H, ^3J = 8.4 Hz, ^4J = 1.8 Hz), 8.02 (brs, 3 H), 8.03 (d, 1H, ^4J = 1.8 Hz), 8.49 (s, 1 H). ^{13}C NMR (75 MHz, DMSO-d_6): δ 14.6 (CH_3), 24.5 (CH_2), 26.8 (CH_2), 38.6 (CH_2), 51.6 (CH_2), 60.3 (CH_2), 111.1 (C_{IV}), 129.5 (CH), 130.5 (CH), 131.0 (CH), 131.3 (C_{IV}), 133.4 (C_{IV}), 137.2 (C_{IV}), 137.4 (CH), 119.3 (C_{IV}), 162.8 (CO). LC-MS (ESI): *m/z* Calculated: 355.09, Found: 356.10, $[M+H]^+$, t_R = 2.5 min.

1-(2-Aminoethyl)-*N*-benzyl-3-(3,4-dichlorophenyl)-1*H*-pyrazole-4-carboxamide (7). Following the general procedure, the compound **7** was isolated by FC (70 mg, 27 %); ^{1}H NMR (300 MHz, $(CD_3)_2CO$): δ 3.63 (t, 2 H, ^3J = 6.1 Hz), 4.38 (t, 2 H, ^3J = 6.1 Hz), 4.51 (d, 2 H, ^3J = 6.0 Hz), 7.28 (m, 5 H), 7.52 (d, 1 H, ^3J = 8.4 Hz), 7.75 (brs, 1 H), 7.86 (dd, 1 H, ^3J = 8.4 Hz, ^4J = 2.0 Hz), 8.17 (s, 1 H), 8.18 (d, 1 H, ^4J = 2.0 Hz). ^{13}C NMR (75 MHz, $(CD_3)_2CO$): δ 42.6 (CH_2), 50.6 (CH_2), 53.4 (CH_2), 126.8 (CH), 127.5 (2 CH), 128.3 (2 CH),

128.5 (CH), 129.8 (CH), 130.4 (CH), 130.8 (C_{IV}), 131.1 (C_{IV}), 133.2 (CH), 133.3 (C_{IV}), 134.2 (C_{IV}), 139.7 (C_{IV}), 147.6 (C_{IV}), 162.8 (CO). LC-MS (ESI): *m/z* Calculated: 388.08, Found: 389.20, $[M+H]^+$, t_R = 2.5 min.

1-(3-Aminopropyl)-*N*-benzyl-3-(3,4-dichlorophenyl)-1*H*-pyrazole-4-carboxamide (8). Following the general procedure, the compound **8** was isolated by FC (220 mg, 97 %); ^{1}H NMR (300 MHz, CD_2Cl_2): δ 2.00 (m, 2 H), 2.72 (t, 2 H, ^3J = 6.6 Hz), 4.26 (t, 2 H, ^3J = 6.9 Hz), 4.51 (d, 2 H, ^3J = 5.8 Hz), 6.02 (t, 1 H, ^3J = 5.8 Hz), 7.25-7.93 (m, 5 H), 7.45 (d, 1 H, ^3J = 8.3 Hz), 7.59 (dd, 1 H, ^3J = 8.3 Hz, ^4J = 2.0 Hz), 7.89 (d, 1 H, ^4J = 2.0 Hz), 7.90 (s, 1 H). ^{13}C NMR (75 MHz, CD_2Cl_2): δ 33.3 (CH_2), 38.7 (CH_2), 43.5 (CH_2), 50.0 (CH_2), 115.8 (C_{IV}), 127.4 (CH), 127.6 (2 CH), 128.2 (CH), 128.6 (2 CH), 130.3 (CH), 130.5 (CH), 132.2 (C_{IV}), 132.3 (C_{IV}), 132.6 (CH), 133.0 (C_{IV}), 138.4 (C_{IV}), 147.4 (C_{IV}), 162.7 (CO). LC-MS (ESI): *m/z* Calculated: 402.10, Found: 403.20, $[M+H]^+$, t_R = 2.5 min.

1-(4-Aminobutyl)-*N*-benzyl-3-(3,4-dichlorophenyl)-1*H*-pyrazole-4-carboxamide (9). Following the general procedure, the compound **9** was isolated by FC (45 mg, 66 %); ^{1}H NMR (300 MHz, $(CD_3)_2CO$): δ 1.63 (quint, 2 H), 1.98 (m, 2 H), 3.25 (t, 2 H, ^3J = 6.7 Hz), 4.25 (t, 2 H, ^3J = 7.0 Hz), 4.52 (d, 2 H), 7.15-7.42 (m, 5 H), 7.54 (d, 1 H, ^3J = 8.4 Hz), 7.93 (dd, 1 H, ^3J = 8.4 Hz, ^4J = 2.0 Hz), 8.23 (d, 2 H), 8.25 (s, 1 H). ^{13}C NMR (75 MHz, DMSO-d_6): δ 26.8 (CH_2), 27.4 (CH_2), 38.8 (CH_2), 40.0 (CH_2), 51.4 (CH_2), 115.2 (C_{IV}), 126.7 (CH), 127.3 (2 CH), 128.3 (C_{IV}), 128.4 (2 CH), 128.5 (C_{IV}), 129.9 (CH), 130.0 (CH),

130.5 (CH), 133.1 (CH), 133.7 (C_{IV}), 139.6 (C_{IV}), 147.0 (C_{IV}), 162.7 (CO). LC-MS (ESI): *m/z* Calculated: 416.12, Found: 417.30, $[M+H]^+$, t_R = 2.5 min.

1-(2-Aminoethyl)-3-(3,4-dichlorophenyl)-*N*-phenethyl-1*H*-pyrazole-4-carboxamide (10). Following the general procedure, the compound **10** was isolated by FC (9 mg, 22 %); ^{1}H NMR (300 MHz, DMSO-d_6): δ 2.81 (t, 2 H, ^3J = 6.9 Hz), 3.09 (t, 2 H, ^3J = 6.1 Hz), 3.42 (t, 2 H, ^3J = 6.5 Hz), 4.16 (t, 2 H, ^3J = 6.1 Hz), 7.20-7.32 (m, 5 H), 7.61 (d, 1 H, ^3J = 8.4 Hz), 7.73 (dd, 1 H, ^3J = 8.4 Hz, ^4J = 2.0 Hz), 8.08 (s, 1 H), 8.16 (d, 1 H, ^4J = 2.0 Hz), 8.23 (t, 1 H). ^{13}C NMR (75 MHz, DMSO-d_6): δ 35.6 (CH_2), 40.7 (CH_2), 41.7 (CH_2), 54.9(CH_2), 115.9 (C_{IV}), 126.6 (CH), 127.7 (2 CH), 128.8 (2 CH), 129.1 (CH), 130.3 (CH), 130.5 (CH), 130.6 (C_{IV}), 131.0 (C_{IV}), 133.0 (CH), 134.1 (C_{IV}), 139.9 (C_{IV}), 147.4 (C_{IV}), 163.1 (CO). LC-MS (ESI): *m/z* Calculated: 402.10, Found: 403.20, $[M+H]^+$, t_R = 2.6 min.

1-(3-Aminopropyl)-3-(3,4-dichlorophenyl)-*N*-phenethyl-1*H*-pyrazole-4-carboxamide (11). Following the general procedure, the compound **11** was isolated by FC (240 mg, 63 %); ^{1}H NMR (300 MHz, DMSO-d_6): δ 1.90 (m, 2H); 2.81 (t, 2 H, ^3J = 7.0 Hz), 3.19 (brs, 2 H), 3.42 (m, 2 H), 4.22 (t, 2 H, ^3J = 7.0 Hz), 7.19-7.26 (m, 5 H), 7.30 (d, 1 H, ^3J = 8.4 Hz), 7.72 (dd, 1 H, ^3J = 8.4 Hz, ^4J = 2.0 Hz); 8.05 (s, 1 H), 8.17 (d, 1 H, ^4J = 2.0 Hz), 8.25 (brs, 1 H). ^{13}C NMR (75 MHz, DMSO-d_6): δ 26.5 (CH_2), 35.6 (CH_2), 40.6 (CH_2), 47.4 (CH_2), 49.9 (CH_2), 115.9 (C_{IV}), 126.6 (CH), 128.7 (2 CH), 128.8 (CH), 129.1 (2 CH), 130.2 (CH), 130.5 (CH), 130.6 (C_{IV}), 131.0 (C_{IV}), 133.2 (CH), 134.2 (C_{IV}),

139.9 (C_{IV}), 147.2 (C_{IV}), 163.1 (CO); LC-MS (ESI): *m/z* Calculated: 416.12, Found: 417.10, $[M+H]^+$, t_R = 2.4 min.

1-(4-Aminobutyl)-3-(3,4-dichlorophenyl)-*N*-phenethyl-1*H*-pyrazole-4-carboxamide (12). Following the general procedure, the compound **12** was isolated by FC (13 mg, 72 %); ^{1}H NMR (300 MHz, DMSO-d_6): δ 1.56 (quint, 2 H, ^3J = 7.0 Hz), 1.88 (m, 2 H), 2.82 (m, 2 H), 3.43 (m, 4 H), 4.20 (t, 2 H, ^3J = 7.0 Hz), 7.11-7.31 (m, 5 H), 7.63 (d, 1 H, ^3J = 8.5 Hz), 7.74 (dd, 1 H, ^3J = 8.5 Hz, ^4J = 2.0 Hz), 7.92 (brs, 1 H), 8.06 (d, 1 H, ^4J = 2.0 Hz), 8.23 (s, 1 H), 8.33 (t, 1 H). ^{13}C NMR (75 MHz, DMSO-d_6): δ 24.2(CH_2), 26.5 (CH_2), 35.2 (CH_2), 40.6 (CH_2), 42.4 (CH_2), 51.1 (CH_2), 115.6 (C_{IV}), 126.1 (CH), 128.3 (2 CH), 128.6 (2 CH), 129.7 (C_{IV}), 130.1 (CH), 130.3 (CH), 130.6 (CH), 130.65 (C_{IV}), 132.9 (CH), 133.6 (C_{IV}), 139.4 (C_{IV}), 146.9 (C_{IV}), 162.6 (CO). LC-MS (ESI): *m/z* Calculated: 430.13, Found: 431.20, $[M+H]^+$, t_R = 3.3 min.

General procedure for the synthesis of [4-(benzylcarbamoyl)-3-(3,4-dichlorophenyl)-1*H*-pyrazol-1-yl]alkanoic acids.

Ethyl [4-(benzylcarbamoyl)-3-(3,4-dichlorophenyl)-1*H*-pyrazol-1-yl]alkanoates. A solution of *N*-benzyl or phenethyl-5-(3,4-dichlorophenyl)-1*H*-pyrazole-4-carboxamide (1 eq., 0.30 g, 0.87 mmol), K_2CO_3 (2 eq., 0.24 g, 1.73 mmol) and the convenient ethyl ω-bromoalkylcarboxylate (1 eq., 0.87 mmol) in anhydrous acetonitrile (15 mL) and under a nitrogen atmosphere was stirred at reflux overnight and concentrated under reduced pressure. The residue was

taken up in EtOAc and washed with water. The organic layer was dried over $MgSO_4$, concentrated under vacuum and purified by FC (DCM/MeOH 98/2).

[4-(Benzylcarbamoyl)-3-(3,4-dichlorophenyl)-1*H*-pyrazol-1-yl]alkanoic acids. A solution of ethyl [4-(benzylcarbamoyl)-3-(3,4-dichlorophenyl)-1*H*-pyrazol-1-yl]alkanoate (1 eq., 0.15 mmol) and NaOH (10 eq., 1.52 mmol) in EtOH (2 mL) was stirred at reflux for 16 h and concentrated under reduced pressure. The residue was taken up in water and extracted with DCM. The aqueous layer was acidified with aq. 1.0 M HCl solution and extracted with EtOAc. The organic phase was dried over magnesium sulfate and concentrated under vacuum to afford **13-16**.

3-(4-(Benzylcarbamoyl)-3-(3,4-dichlorophenyl)-1*H*-pyrazol-1-yl)propanoic acid (13). Following the general procedure, the ester was obtained in a 52 % yield and immediately converted into its acid. Compound **13** was isolated (26 mg, 43%); ^{1}H NMR (300 MHz, DMSO-d_6): δ 2.85 (t, 2 H, J = 6.6 Hz), 4.37 (m, 4 H), 7.28 (m, 5 H), 7.61 (d, 1 H, ^3J = 8.4 Hz), 7.76 (dd, 1 H, ^3J = 8.4 Hz, ^4J = 2.0 Hz), 8.04 (d, 1 H, ^4J = 2.0 Hz), 8.28 (s, 1 H), 8.66 (t, 1 H, ^3J = 5.7 Hz, NH), 12.41 (brs, 1 H). ^{13}C NMR (75 MHz, DMSO-d_6): δ 34.6 (CH_2), 42.7 (CH_2), 48.2 (CH_2), 115.6 (C_{IV}), 127.2 (CH), 127.7 (2 CH), 128.8 (2 CH), 128.9 (CH), 130.4 (CH), 130.5 (CH), 130.7 (C_{IV}), 130.9 (C_{IV}), 131.0 (C_{IV}), 133.7 (CH), 134.1 (C_{IV}), 147.6 (C_{IV}), 160.0 (CO), 172.7 (CO); LC-MS (ESI): *m/z* Calculated: 417.27, Found: 418.30, $[M+H]^+$, t_R = 2.5 min.

4-(4-(Benzylcarbamoyl)-3-(3,4-dichlorophenyl)-1*H*-pyrazol-1-yl)butanoic acid (14). Following the general procedure, the ester was obtained in a 23% yield and immediately converted into its acid. Compound **14** was isolated (57 mg, 91 %); ^{1}H NMR (300 MHz, DMSO-d_6): δ 2.03 (m, 2 H), 2.26 (t, 2 H, ^{3}J = 7.1 Hz), 4.18 (t, 2 H, ^{3}J = 6.9 Hz), 4.39 (d, 2 H, ^{3}J = 5.9 Hz), 7.30 (m, 5 H), 7.61 (d, 1 H, ^{3}J = 8.3 Hz), 7.77 (dd, 1 H, ^{3}J = 8.4 Hz, ^{4}J = 2.0 Hz), 8.06 (d, 1 H, ^{4}J = 2.0 Hz), 8.27 (s, 1 H), 8.66 (t, 1 H, ^{3}J = 5.9 Hz, NH), 12.19 (brs, 1 H, OH). ^{13}C NMR (75 MHz, DMSO-d_6): δ 25.5 (CH_2), 30.9 (CH_2), 42.7 (CH_2), 51.4 (CH_2), 115.7 (C_{IV}) 127.2 (CH), 127.7 (2 CH), 128.7 (2 CH), 128.9 (CH), 130.4 (CH), 130.5 (CH), 130.7 (C_{IV}), 130.9 (C_{IV}), 133.5 (CH), 134.1 (C_{IV}), 140.0 (C_{IV}), 147.5 (C_{IV}), 163.1 (CO), 174.2 (CO); LC-MS (ESI): *m/z* Calculated: 431.30, Found: 432.20, $[M+H]^+$, t_R = 2.8 min.

3-(3-(3,4-Dichlorophenyl)-4-(phenethylcarbamoyl)-1*H*-pyrazol-1-yl)propanoic acid (15). Following the general procedure, the ester was obtained in a 52 % yield and immediately converted into its acid. Compound **15** was isolated (40 mg, 64%); ^{1}H NMR (300 MHz, DMSO-d_6): δ 2.68 (t, 2 H, ^{3}J = 6.9 Hz), 2.80 (t, 2 H, ^{3}J = 7.0 Hz), 3.39 (q, 2 H, ^{3}J = 6.9 Hz), 4.30 (t, 2 H, ^{3}J = 6.7 Hz), 7.14-7.32 (m, 5 H), 7.60 (d, 1 H, ^{3}J = 8.4 Hz), 7.71 (dd, 1H, ^{3}J = 8.4 Hz, ^{4}J = 2.0 Hz), 8.02 (d, 1 H, ^{3}J = 2.0 Hz), 8.16 (s, 1 H), 8.21 (t, 1 H, ^{3}J = 5.7 Hz, NH). ^{13}C NMR (75 MHz, DMSO-d_6): δ 34.3 (CH_2), 35.6 (CH_2), 49.2 (CH_2), 62.2 (CH_2), 116.1 (C_{IV}), 126.5 (CH), 128.0 (CH), 128.8 (2 CH), 129.1 (2 CH), 130.3 (CH), 130.5 (CH), 130.9 (C_{IV}), 132.3 (C_{IV}), 132.8 (C_{IV}), 133.4 (CH),

139.9 (C_{IV}), 146.0 (C_{IV}), 163.0 (CO), 170.2 (CO); LC-MS (ESI): *m/z* Calculated: 431.30, Found: 432.20, $[M+H]^+$, t_R = 2.8 min.

4-(3-(3,4-Dichlorophenyl)-4-(phenethylcarbamoyl)-1*H*-pyrazol-1-yl)butanoic acid (16). Following the general procedure, the ester was obtained in a 52% yield and immediately converted into its acid. Compound **16** was isolated (36 mg, 56%); ^{1}H NMR (300 MHz, $(CD_3)_2CO$): δ 2.02 (m, 2 H), 2.24 (t, 2 H, ^3J = 6.8 Hz), 2.77 (t, 2 H, ^3J = 7.1 Hz), 3.44 (m, 2 H), 4.07 (t, 2 H, ^3J = 7.0 Hz), 7.08 (brs, 1 H), 7.12-7.30 (m, 5 H), 7.39 (dd, 1 H, ^3J = 8.2 Hz, ^4J = 2.0 Hz), 7,65 (d, 1 H, ^3J = 8.2 Hz), 7.67 (d, 1 H, ^4J = 2.0 Hz), 7.88 (s, 1 H). ^{13}C NMR (75 MHz, $(CD_3)_2CO$): δ 24.9 (CH_2), 35.6 (CH_2), 40.3 (CH_2), 40.4 (CH_2), 48.3 (CH_2), 116.9 (C_{IV}), 126.1 (CH), 128.3 (2 CH), 128.6 (2 CH), 130.2 (C_{IV}), 130.3 (CH), 130.4 (CH), 131.7 (C_{IV}), 132.4 (CH), 132.6 (C_{IV}), 138.1 (CH), 139.6 (C_{IV}), 141.0 (C_{IV}), 161.8 (CO), 172.9 (CO). LC-MS (ESI): *m/z* Calculated: 445.10, Found: 446.20, $[M+H]^+$, t_R = 2.7 min.

Protein expression and purification. The human TEAD2 sequence (residue 217 to 447) was expressed and purified according to [34].

Crystallization and structure determination. Crystals of $hTEAD2_{217–447}$ were grown at 20 °C using the hanging-drop vapor-diffusion method with a reservoir solution containing 0.1 M HEPES (pH 7.2) and 2.8 M sodium formate. The crystals were cryo-protected with reservoir solution supplemented with 25 % glycerol and then flash-cooled in liquid nitrogen. X-ray diffraction data were collected at the ALBA Synchrotron in Barcelona, Spain, on beamline BL13-

XALOC. Data were integrated and processed using XDS [51]. The crystals belong to the space group C2 with two monomers in the asymmetric unit. The structures were solved by molecular replacement using PDB entry 5EMV as the search model. Bound ligands were manually identified and fitted into Fo–Fc electron density using Coot [52]. Files CIF format for ligand were generated using Grade Server (http://grade.globalphasing.org/cgi-bin/grade/server.cgi). The structures were refined by rounds of rebuilding in Coot and refinement using Phenix [53]. Data collection and refinement statistics for crystal structures are presented in Supplement Tables 1 and 2.

NanoDSF Assay. NanoDSF assay were conducted according to [34].

Microscale Thermophoresis. Microscale Thermophoresis experiments were conducted according to [33].

Cell Cultures. Cell cultures were made according to [33]

Luciferase Reporter Assay. Luciferase reporter assay was made as described in [34].

Western blotting.

The MDA-MB-231 cell line was cultivated in DMEM media containing 0.2 % heat-inactivated fetal bovine serum (FBS), L-glutamine (2 mM), and penicillin/streptomycin (100 $U.mL^{-1}$/0.1 $mg.mL^{-1}$). Total extracts of cells were obtained with a RIPA based buffer containing protease and phosphatase

inhibitors (Roche). Western blots were carried out using 20 mg of protein lysates with the NuPage Electrophoresis and Iblot transfer systems (Life Technologies). GADPH was used as loading control for total extracts.

Kinetic Cell Growth Assay

The effect of **6** on MDA-MB-231 cell growth was studied using a kinetic cell growth assay. MDA-MB-231 cells were plated on 96-well TPP plates in triplicate at low densities (2.5 x 10^3 cells/well) in low serum conditions (0.2 % SVF). **6** at different concentrations was added 24 h after plating and cell number was monitored with Incucyte Live-Cell imaging System and software (Essen Instruments). Cell number was observed every 3 h for 72 h. The assay was performed in independent triplicates.

RNA Extraction and Quantitative RT-PCR

After the treatment of the MDA cells with DMSO (negative control), Dasatinib (positive control) and compound **6** (tested drug), total RNA was purified using NucleoSpin RNA followed by NucleoSpin RNA Clean-up XS2 step (Macherey-Nagel). The integrity of the extracted RNA was tested by using 1 % w/v agarose gel electrophoresis visualized by ethidium bromide staining. 250 ng RNA was reverse-transcribed into cDNA using High-Capacity cDNA Reverse Transcription Kit (Life Technologies) in accordance to the manufacturer's instructions. Quantitative RT-PCR was executed using PowerUP SYBR Green (Thermo Fisher Scientific) 1µL of the reverse-transcript was added to a 10 µL

PCR mixture for 40 cycles. Each cycle included 95 °C for 15 s, 10 cycles of Touch Down PCR from 70 °C to 60 °C for 15 s, and 72 °C for 30 s, followed by 30 cycles of 60 °C for 15 s and 72 °C for 30 s, to conclude with 5 min at 72 °C. PCR amplicons were run in 3 % w/v agarose gel electrophoresis and visualized by ethidium bromide staining. The primers for AXL were designed by using Oligo 7 (version 7.60) and sequence specificity checked using-BLAST software, the primers for CTGF were taken from Nagaraja *et al*. [54] and Cyr61 from Chen *et al.* [55]. They were manufactured by Eurogentec. Primer sequences are listed below. The relative expression value of each target gene (AXL, CTGF and Cyr61) was utilizing the $2^{-\Delta\Delta CT}$ method using MAN2B1 for normalization. All experiments were performed at least in triplicates.

	Primers	
	Forward	Reverse
AXL	5'-GGAGCCCAACAACTTCTGAGG-3'	5'-GGACTTTCTTCAGCCTGCGTG-3'
CTGF	5’-AATGCTGCGAGGAGTGGGT-3’	5’-GGCTCTAATCATAGTTGGGTCT-3’
Cyr61	5’-GAGTGGGTCTGTGACGAGGAT-3’	5’-GGTTGTATAGGATGCGAGGCT-3’

AUTHOR INFORMATION

Corresponding Authors *

Jean-François Guichou: Phone: +33-4-6741-7712. E-mail: guichou@cbs.cnrs.fr

Philippe Cotelle: Phone: +33-3-6228-3694. E-mail: philippe.cotelle@univ-lille.fr

ORCID

Manon Sturbaut: 0000-0002-4026-2211

Fabrice Bailly: 0000-0001-9681-9309

Mathilde Coevoet : 0000-0001-7529-6676

Pasquale Sileo : 0000-0001-9991-7430

Maxime Liberelle: 0000-0002-8620-9256

Martine Pugnière: 0000-0002-2049-2909

Xavier Thuru: 0000-0002-0998-4160

Patricia Melnyk: 0000-0002-9555-3446

Marie-Christine Chartier-Harlin: 0000-0001-6416-6526

Muriel Gelin: 0000-0003-1320-8663

Frédéric Allemand: 0000-0003-0396-6145

Jean-François Guichou: 0000-0002-7699-3235

Philippe Cotelle: 0000-0003-0924-0433

Author Contributions

M.S. took part in all the described experiments; F.B. supervised the chemical synthesis; M.C. performed most of the biological assays; P. S. performed RT-qPCR measurements; M.P. performed NanoDSF experiments; M.L., R.M. and X.T. helped at the expression of GFP-TEAD2 in CHO cells; M.G. and F.A. produced and purified hTEAD2$_{217–447}$ protein and performed crystallization and structure determination; J.-F.G. supervised all the X-ray crystallography,

NanoDSF studies; J.-F.G., P.M., and P.C. co-supervised all the project; P.C. supervised writing the article.

Notes

The authors declare no competing financial interest.

ACKNOWLEDGMENTS

This work was financially supported by grants from le Ministère de l'Education et de la Recherche and the University of Lille (M. S. and P.S.) and fundings from le Cancéropôle Nord-Ouest (Mobility Support Program for Young Researchers, M. S.). We express our thanks to the NMR facility (Lille University), the Region Hauts-de-France (France), the Ministère de la Jeunesse, de l'Education Nationale et de la Recherche (MJENR) and the Fonds Européens de Développement Régional (FEDER) and the Lille University Molecular Interactions facility. This work was also supported by the French Infrastructure for Integrated Structural Biology (FRISBI) ANR-10-INSB-05-01. These experiments were performed at BL13-XALOC beamline at ALBA Synchrotron with the collaboration of ALBA staff.

ABBREVIATIONS

CTGF, connective tissue growth factor; Cyr61, cysteine-rich angiogenic protein; DMF-DMA *N,N*-dimethylformamide dimethylacetal; nano-DSF, differential

scanning fluorimetry; EDCI, *N*-(3-dimethylaminopropyl)-*N′*-ethylcarbodiimide hydrochloride; HOBt, 1-hydroxybenzotriazole; Lats1/2, large tumor suppressor kinase; Mob, mps one binder kinase; MST, microscale thermophoresis; Mst1/2, mammalian ste20-like protein kinase; Nif Ac. niflumic acid; Sav1, scaffold protein Salvador; TAZ, transcriptional coactivator with PDZ-binding motif; TBD, TEAD binding domain; TEAD, transcriptional enhanced associated domain; TSA, thermal shift assay; VGLL (Transcriptional cofactor Vestigial like protein family); YAP, Yes associated protein; Y/TBD, YAP/TAZ binding domain.

ACCESSION NUMBERS

The atomic coordinates and structure factors for hTEAD2-**6**, hTEAD2-**7**, hTEAD2-**13**, hTEAD2-**14**, and hTEAD2-**15** have been deposited in the PDB with the codes PDB: 6S6J, 6S66, 6S64, 6S60 and 5S69, respectively. Authors will release the atomic coordinates and experimental data upon article publication.

REFERENCES

[1] Piccolo, S.; Dupont, S.; Cordenonsi, M. The Biology of YAP/TAZ: Hippo Signaling and Beyond. *Physiol. Rev.* **2014**, *94*, 1287–1312. https://doi.org/10.1152/physrev.00005.2014.

[2] Pobbati, A. V.; Hong, W. Emerging Roles of TEAD Transcription Factors and Its Coactivators in Cancers. *Cancer Biol. Ther.* **2013**, *14*, 390–398. https://doi.org/10.4161/cbt.23788.

[3] Bokhovchuk, F.; Mesrouze, Y.; Delaunay, C.; Martin, T.; Villard, F.; Meyerhofer, M.; Fontana, P.; Zimmermann, C.; Erdmann, D.; Furet, P.; Scheufler, C.; Schmelzle, T.; Chène, P. Identification of FAM181A and FAM181B as New Interactors with the TEAD Transcription Factors. *Protein Sci. Publ. Protein Soc.* **2020**, *29*, 509–520. https://doi.org/10.1002/pro.3775.

[4] Marks, M.; Pennimpede, T.; Lange, L.; Grote, P.; Herrmann, B. G.; Wittler, L. Analysis of the Fam181 Gene Family during Mouse Development Reveals Distinct Strain-Specific Expression Patterns, Suggesting a Role in Nervous System Development and Function. *Gene* **2016**, *575*, 438–451. https://doi.org/10.1016/j.gene.2015.09.035.

[5] Lin, K. C.; Park, H. W.; Guan, K.-L. Regulation of the Hippo Pathway Transcription Factor TEAD. *Trends Biochem. Sci.* **2017**, *42*, 862–872. https://doi.org/10.1016/j.tibs.2017.09.003.

[6] Wang, Y.; *et al.* Comprehensive Molecular Characterization of the Hippo Signaling Pathway in Cancer. *Cell Rep.* **2018**, *25*, 1304-1317.e5. https://doi.org/10.1016/j.celrep.2018.10.001.

[7] Dey, A.; Varelas, X.; Guan, K.-L. Targeting the Hippo Pathway in Cancer, Fibrosis, Wound Healing and Regenerative Medicine. *Nat. Rev. Drug Discov.* **2020***, 19,* 480-494. https://doi: 10.1038/s41573-020-0070-z.

[8] Li, Z.; Zhao, B.; Wang, P.; Chen, F.; Dong, Z.; Yang, H.; Guan, K.-L.; Xu, Y. Structural Insights into the YAP and TEAD Complex. *Genes Dev.* **2010**, *24*, 235–240. https://doi.org/10.1101/gad.1865810.

[9] Hau, J. C.; Erdmann, D.; Mesrouze, Y.; Furet, P.; Fontana, P.; Zimmermann, C.; Schmelzle, T.; Hofmann, F.; Chène, P. The TEAD4-YAP/TAZ Protein-Protein Interaction: Expected Similarities and Unexpected Differences. *ChemBioChem* **2013**, *14*, 1218–1225. https://doi.org/10.1002/cbic.201300163.

[10] Bokhovchuk, F.; Mesrouze, Y.; Izaac, A.; Meyerhofer, M.; Zimmermann, C.; Fontana, P.; Schmelzle, T.; Erdmann, D.; Furet, P.; Kallen, J.; Chène, P. Molecular and Structural Characterization of a TEAD Mutation at the Origin of Sveinsson's Chorioretinal Atrophy. *FEBS J.* **2019**, *286*, 2381–2398. https://doi.org/10.1111/febs.14817.

[11] Bokhovchuk, F.; Mesrouze, Y.; Meyerhofer, M.; Zimmermann, C.; Fontana, P.; Erdmann, D.; Jemth, P.; Chène, P. An Early Association between the α-Helix of the TEAD Binding Domain of YAP and TEAD Drives the Formation of the YAP:TEAD Complex. *Biochemistry* **2020**, *59*, 1804–1812. https://doi.org/10.1021/acs.biochem.0c00217.

[12] Gibault, F.; Sturbaut, M.; Bailly, F.; Melnyk, P.; Cotelle, P. Targeting Transcriptional Enhanced Associate Domains (TEADs). *J. Med. Chem.* **2018**, *61*, 5057–5072. https://doi.org/10.1021/acs.jmedchem.7b00879.

[13] Noland, C. L.; Gierke, S.; Schnier, P. D.; Murray, J.; Sandoval, W. N.; Sagolla, M.; Dey, A.; Hannoush, R. N.; Fairbrother, W. J.; Cunningham,

C. N. Palmitoylation of TEAD Transcription Factors Is Required for Their Stability and Function in Hippo Pathway Signaling. *Structure* **2016**, *24*, 179–186. https://doi.org/10.1016/j.str.2015.11.005.

[14] Chan, P.; Han, X.; Zheng, B.; DeRan, M.; Yu, J.; Jarugumilli, G. K.; Deng, H.; Pan, D.; Luo, X.; Wu, X. Autopalmitoylation of TEAD Proteins Regulates Transcriptional Output of the Hippo Pathway. *Nat. Chem. Biol.* **2016**, *12*, 282–289. https://doi.org/10.1038/nchembio.2036.

[15] Song, J.; Gao, Q.-L.; Wu, B.-W.; Zhu, T.; Cui, X.-X.; Jin, C.-J.; Wang, S.-Y.; Wang, S.-H.; Fu, D.-J.; Liu, H.-M.; Zhang, S.-Y.; Zhang, Y.-B.; Li, Y.-C. Discovery of Tertiary Amide Derivatives Incorporating Benzothiazole Moiety as Anti-Gastric Cancer Agents in Vitro via Inhibiting Tubulin Polymerization and Activating the Hippo Signaling Pathway. *Eur J Med Chem* **2020**, *203*, 112618. https://doi.org/10.1016/j.ejmech.2020.112618.

[16] Pobbati, A. V.; Hong, W. A Combat with the YAP/TAZ-TEAD Oncoproteins for Cancer Therapy. *Theranostics* **2020**, *10*, 3622–3635. https://doi.org/10.7150/thno.40889.

[17] Zhang, Z.; Lin, Z.; Zhou, Z.; Shen, H. C.; Yan, S. F.; Mayweg, A. V.; Xu, Z.; Qin, N.; Wong, J. C.; Zhang, Z.; Rong, Y.; Fry, D. C.; Hu, T. Structure-Based Design and Synthesis of Potent Cyclic Peptides Inhibiting the YAP–TEAD Protein–Protein Interaction. *ACS Med. Chem. Lett.* **2014**, *5*, 993–998. https://doi.org/10.1021/ml500160m.

[18] Jiao, S.; Wang, H.; Shi, Z.; Dong, A.; Zhang, W.; Song, X.; He, F.; Wang, Y.; Zhang, Z.; Wang, W.; Wang, X.; Guo, T.; Li, P.; Zhao, Y.; Ji, H.; Zhang, L.; Zhou, Z. A Peptide Mimicking VGLL4 Function Acts as a YAP Antagonist Therapy against Gastric Cancer. *Cancer Cell* **2014**, *25*, 166–180. https://doi.org/10.1016/j.ccr.2014.01.010.

[19] Zhou, Z.; Hu, T.; Xu, Z.; Lin, Z.; Zhang, Z.; Feng, T.; Zhu, L.; Rong, Y.; Shen, H.; Luk, J. M.; Zhang, X.; Qin, N. Targeting Hippo Pathway by Specific Interruption of YAP-TEAD Interaction Using Cyclic YAP-like Peptides. *FASEB J.* **2015**, *29*, 724–732. https://doi.org/10.1096/fj.14-262980.

[20] Smith, S. A.; Sessions, R. B.; Shoemark, D. K.; Williams, C.; Ebrahimighaei, R.; McNeill, M. C.; Crump, M. P.; McKay, T. R.; Harris, G.; Newby, A. C.; Bond, M. Antiproliferative and Antimigratory Effects of a Novel YAP-TEAD Interaction Inhibitor Identified Using in Silico Molecular Docking. *J. Med. Chem.* **2019**, *62*, 1291–1305. https://doi.org/10.1021/acs.jmedchem.8b01402.

[21] Pobbati, A. V.; Han, X.; Hung, A. W.; Weiguang, S.; Huda, N.; Chen, G.-Y.; Kang, C.; Chia, C. S. B.; Luo, X.; Hong, W.; Poulsen, A. Targeting the Central Pocket in Human Transcription Factor TEAD as a Potential Cancer Therapeutic Strategy. *Structure* **2015**, *23*, 2076–2086. https://doi.org/10.1016/j.str.2015.09.009

[22] Bum-Erdene, K.; Zhou, D.; Gonzalez-Gutierrez, G.; Ghozayel, M. K.; Si, Y.; Xu, D.; Shannon, H. E.; Bailey, B. J.; Corson, T. W.; Pollok, K. E.; Wells, C. D.; Meroueh, S. O. Small-Molecule Covalent Modification of Conserved Cysteine Leads to Allosteric Inhibition of the TEAD·Yap Protein-Protein Interaction. *Cell Chem. Biol.* **2019**, *26*, 378-389.e13. https://doi.org/10.1016/j.chembiol.2018.11.010.

[23] Kurppa, K. J.; Liu, Y.; To, C.; Zhang, T.; Fan, M.; Vajdi, A.; Knelson, E. H.; Xie, Y.; Lim, K.; Cejas, P.; Portell, A.; Lizotte, P. H.; Ficarro, S. B.; Li, S.; Chen, T.; Haikala, H. M.; Wang, H.; Bahcall, M.; Gao, Y.; Shalhout, S.; Boettcher, S.; Shin, B. H.; Thai, T.; Wilkens, M. K.; Tillgren, M. L.; Mushajiang, M.; Xu, M.; Choi, J.; Bertram, A. A.; Ebert, B. L.; Beroukhim, R.; Bandopadhayay, P.; Awad, M. M.; Gokhale, P. C.; Kirschmeier, P. T.; Marto, J. A.; Camargo, F. D.; Haq, R.; Paweletz, C. P.; Wong, K.-K.; Barbie, D. A.; Long, H. W.; Gray, N. S.; Jänne, P. A. Treatment-Induced Tumor Dormancy through YAP-Mediated Transcriptional Reprogramming of the Apoptotic Pathway. *Cancer Cell* **2020**, *37*, 104-122.e12. https://doi.org/10.1016/j.ccell.2019.12.006.

[24] Lu, W.; Wang, J.; Li, Y.; Tao, H.; Xiong, H.; Lian, F.; Gao, J.; Ma, H.; Lu, T.; Zhang, D.; Ye, X.; Ding, H.; Yue, L.; Zhang, Y.; Tang, H.; Zhang, N.; Yang, Y.; Jiang, H.; Chen, K.; Zhou, B.; Luo, C. Discovery and Biological Evaluation of Vinylsulfonamide Derivatives as Highly Potent, Covalent TEAD Autopalmitoylation Inhibitors. *Eur J Med Chem* **2019**, *184*, 111767. https://doi.org/10.1016/j.ejmech.2019.111767.

[25] Kaneda, A.; Seike, T.; Danjo, T.; Nakajima, T.; Otsubo, N.; Yamaguchi, D.; Tsuji, Y.; Hamaguchi, K.; Yasunaga, M.; Nishiya, Y.; Suzuki, M.; Saito, J.-I.; Yatsunami, R.; Nakamura, S.; Sekido, Y.; Mori, K. The Novel Potent TEAD Inhibitor, K-975, Inhibits YAP1/TAZ-TEAD Protein-Protein Interactions and Exerts an Anti-Tumor Effect on Malignant Pleural Mesothelioma. *Am J Cancer Res* **2020**, *10*, 4399–4415.

[26] Li, Q.; Sun, Y.; Jarugumilli, G. K.; Liu, S.; Dang, K.; Cotton, J. L.; Xiol, J.; Chan, P. Y.; DeRan, M.; Ma, L.; Li, R.; Zhu, L. J.; Li, J. H.; Leiter, A. B.; Ip, Y. T.; Camargo, F. D.; Luo, X.; Johnson, R. L.; Wu, X.; Mao, J. Lats1/2 Sustain Intestinal Stem Cells and Wnt Activation through TEAD-Dependent and Independent Transcription. *Cell Stem Cell* **2020**, *26*, 675-.e8. https://doi.org/10.1016/j.stem.2020.03.002.

[27] Wu, X. Tead Transcription Factor Autopalmitoylation Inhibitors. WO2017053706 A1, **2017**.

[28] Holden, J. K.; Crawford, J. J.; Noland, C. L.; Schmidt, S.; Zbieg, J. R.; Lacap, J. A.; Zang, R.; Miller, G. M.; Zhang, Y.; Beroza, P.; Reja, R.; Lee, W.; Tom, J. Y. K.; Fong, R.; Steffek, M.; Clausen, S.; Hagenbeek, T. J.; Hu, T.; Zhou, Z.; Shen, H. C.; Cunningham, C. N. Small Molecule Dysregulation of TEAD Lipidation Induces a Dominant-Negative

Inhibition of Hippo Pathway Signaling. *Cell Rep.* **2020**, *31*, 107809. https://doi.org/10.1016/j.celrep.2020.107809.
[29] Konradi, A.W.; Lin, T. Non-Fused Tricyclic Compounds. WO2018204532: **2018**.
[30] Konradi, A.W.; Lin, T.; Tang, T.T. Preparation of Substituted Naphthalene-2-Carboxamide Derivatives Useful for Treatment of Cancer WO 2020097389 A1 20200514, **2020**
[31] Tang, T. T.; Konradi, A. W.; Feng, Y.; Peng, X.; Ma, M.; Li, J.; Yu, F.-X.; Guan, K.-L.; Post, L. Small Molecule Inhibitors of TEAD Auto-Palmitoylation Selectively Inhibit Proliferation and Tumor Growth of NF2-Deficient Mesothelioma. *Mol Cancer Ther* **2021**. https://doi.org/10.1158/1535-7163.MCT-20-0717.
[32] Kaan, H. Y. K.; Sim, A. Y. L.; Tan, S. K. J.; Verma, C.; Song, H. Targeting YAP/TAZ-TEAD Protein-Protein Interactions Using Fragment-Based and Computational Modeling Approaches. *PLOS ONE* **2017**, *12*, e0178381. https://doi.org/10.1371/journal.pone.0178381.
[33] Gibault, F.; Coevoet, M.; Sturbaut, M.; Farce, A.; Renault, N.; Allemand, F.; Guichou, J.-F.; Drucbert, A.-S.; Foulon, C.; Magnez, R.; Thuru, X.; Corvaisier, M.; Huet, G.; Chavatte, P.; Melnyk, P.; Bailly, F.; Cotelle, P. Toward the Discovery of a Novel Class of YAP–TEAD Interaction Inhibitors by Virtual Screening Approach Targeting YAP–TEAD Protein–Protein Interface. *Cancers* **2018**, *10*, 140. https://doi.org/10.3390/cancers10050140.
[34] Gibault, F.; Sturbaut, M.; Coevoet, M.; Pugnière, M.; Burtscher, A.; Allemand, F.; Melnyk, P.; Hong, W.; Rubin, B.P.; Pobbati, A.V.; Guichou, J.F.; Cotelle, P.; Bailly, F. Design, Synthesis and Evaluation of a Series of 1,5-Diaryl-1,2,3-triazole-4-carbohydrazones as Inhibitors of the YAP-TAZ/TEAD Complex. ChemMedChem. **2021**, May 25. doi: 10.1002/cmdc.202100153.
[35] Šenica, L.; Stopar, K.; Friedrich, M.; Grošelj, U.; Plavec, J.; Počkaj, M.; Podlipnik, Č.; Štefane, B.; Svete, J. Synthesis and Rotational Isomerism of 1-Substituted Methyl (S)-[5-(2-Nitrophenyl)-1H-Pyrazole-4-Carbonyl]Alaninates. *J. Org. Chem.* **2016**, *81*, 146–161. https://doi.org/10.1021/acs.joc.5b02467.
[36] Mesrouze, Y.; Meyerhofer, M.; Bokhovchuk, F.; Fontana, P.; Zimmermann, C.; Martin, T.; Delaunay, C.; Izaac, A.; Kallen, J.; Schmelzle, T.; Erdmann, D.; Chène, P. Effect of the Acylation of TEAD4 on Its Interaction with Co-Activators YAP and TAZ. *Protein Sci. Publ. Protein Soc.* **2017**, *26*, 2399–2409. https://doi.org/10.1002/pro.3312.
[37] Wienken, C. J.; Baaske, P.; Rothbauer, U.; Braun, D.; Duhr, S. Protein-Binding Assays in Biological Liquids Using Microscale Thermophoresis. *Nat. Commun.* **2010**, *1* https://doi.org/10.1038/ncomms1093.

[38] Tian, W.; Yu, J.; Tomchick, D. R.; Pan, D.; Luo, X. Structural and Functional Analysis of the YAP-Binding Domain of Human TEAD2. *Proc. Natl. Acad. Sci.* **2010**, *107*, 7293–7298. https://doi.org/10.1073/pnas.1000293107.

[39] Oku, Y.; Nishiya, N.; Shito, T.; Yamamoto, R.; Yamamoto, Y.; Oyama, C.; Uehara, Y. Small Molecules Inhibiting the Nuclear Localization of YAP/TAZ for Chemotherapeutics and Chemosensitizers against Breast Cancers. *FEBS Open Bio* **2015**, *5*, 542–549. https://doi.org/10.1016/j.fob.2015.06.007.

[40] Pobbati, A. V.; Chan, S. W.; Lee, I.; Song, H.; Hong, W. Structural and Functional Similarity between the Vgll1-TEAD and the YAP-TEAD Complexes. *Struct. Lond. Engl. 1993* **2012**, *20*, 1135–1140. https://doi.org/10.1016/j.str.2012.04.004.

[41] Jiao, S.; Wang, H.; Shi, Z.; Dong, A.; Zhang, W.; Song, X.; He, F.; Wang, Y.; Zhang, Z.; Wang, W.; Wang, X.; Guo, T.; Li, P.; Zhao, Y.; Ji, H.; Zhang, L.; Zhou, Z. A Peptide Mimicking VGLL4 Function Acts as a YAP Antagonist Therapy against Gastric Cancer. *Cancer Cell* **2014**, *25*, 166–180. https://doi.org/10.1016/j.ccr.2014.01.010.

[42] Li, Z.; Zhao, B.; Wang, P.; Chen, F.; Dong, Z.; Yang, H.; Guan, K.-L.; Xu, Y. Structural Insights into the YAP and TEAD Complex. *Genes Dev.* **2010**, *24*, 235–240. https://doi.org/10.1101/gad.1865810.

[43] Gambaro, K.; Quinn, M. C. J.; Wojnarowicz, P. M.; Arcand, S. L.; de Ladurantaye, M.; Barrès, V.; Ripeau, J.-S.; Killary, A. M.; Davis, E. C.; Lavoie, J.; Provencher, D. M.; Mes-Masson, A.-M.; Chevrette, M.; Tonin, P. N. VGLL3 Expression Is Associated with a Tumor Suppressor Phenotype in Epithelial Ovarian Cancer. *Mol. Oncol.* **2013**, *7*, 513–530. https://doi.org/10.1016/j.molonc.2012.12.006.

[44] Deng, X.; Fang, L. VGLL4 Is a Transcriptional Cofactor Acting as a Novel Tumor Suppressor via Interacting with TEADs. *Am. J. Cancer Res.* **2018**, *8*, 932–943.

[45] Castilla, M. Á.; López-García, M. Á.; Atienza, M. R.; Rosa-Rosa, J. M.; Díaz-Martín, J.; Pecero, M. L.; Vieites, B.; Romero-Pérez, L.; Benítez, J.; Calcabrini, A.; Palacios, J. VGLL1 Expression Is Associated with a Triple-Negative Basal-like Phenotype in Breast Cancer. *Endocr. Relat. Cancer* **2014**, *21*, 587–599. https://doi.org/10.1530/ERC-13-0485.

[46] Hallor, K. H.; Sciot, R.; Staaf, J.; Heidenblad, M.; Rydholm, A.; Bauer, H. C.; Aström, K.; Domanski, H. A.; Meis, J. M.; Kindblom, L.-G.; Panagopoulos, I.; Mandahl, N.; Mertens, F. Two Genetic Pathways, t(1;10) and Amplification of 3p11-12, in Myxoinflammatory Fibroblastic Sarcoma, Haemosiderotic Fibrolipomatous Tumour, and Morphologically Similar Lesions. *J. Pathol.* **2009**, *217*, 716–727. https://doi.org/10.1002/path.2513.

[47] Zhang, L.-H.; Wang, Z.; Li, L.-H.; Liu, Y.-K.; Jin, L.-F.; Qi, X.-W.; Zhang, C.; Wang, T.; Hua, D. Vestigial like Family Member 3 Is a Novel Prognostic Biomarker for Gastric Cancer. *World J. Clin. Cases* **2019**, *7*, 1954–1963. https://doi.org/10.12998/wjcc.v7.i15.1954.

[48] Hélias-Rodzewicz, Z.; Pérot, G.; Chibon, F.; Ferreira, C.; Lagarde, P.; Terrier, P.; Coindre, J.-M.; Aurias, A. YAP1 and VGLL3, Encoding Two Cofactors of TEAD Transcription Factors, Are Amplified and Overexpressed in a Subset of Soft Tissue Sarcomas. *Genes. Chromosomes Cancer* **2010**, *49*, 1161–1171. https://doi.org/10.1002/gcc.20825.

[49] Wu, A.; Wu, Q.; Deng, Y.; Liu, Y.; Lu, J.; Liu, L.; Li, X.; Liao, C.; Zhao, B.; Song, H. Loss of VGLL4 Suppresses Tumor PD-L1 Expression and Immune Evasion. *EMBO J.* **2019**, *38*. https://doi.org/10.15252/embj.201899506.

[50] Adihou, H.; Gopalakrishnan, R.; Förster, T.; Guéret, S. M.; Gasper, R.; Geschwindner, S.; Carrillo García, C.; Karatas, H.; Pobbati, A. V.; Vazquez-Chantada, M.; Davey, P.; Wassvik, C. M.; Pang, J. K. S.; Soh, B. S.; Hong, W.; Chiarparin, E.; Schade, D.; Plowright, A. T.; Valeur, E.; Lemurell, M.; Grossmann, T. N.; Waldmann, H. A Protein Tertiary Structure Mimetic Modulator of the Hippo Signalling Pathway. *Nat. Commun.* **2020**, *11*, 5425. https://doi.org/10.1038/s41467-020-19224-8.

[51] Kabsch, W. XDS. *Acta Crystallogr. D Biol. Crystallogr.* **2010**, *66*, 125–132. https://doi.org/10.1107/S0907444909047337.

[52] Emsley, P.; Cowtan, K. Coot: Model-Building Tools for Molecular Graphics. *Acta Crystallogr. D Biol. Crystallogr.* **2004**, *60*, 2126–2132. https://doi.org/10.1107/S09.;7444904019158.

[53] Adams, P.D.; Afonine, P.V.; Bunkóczi, G.; Chen, V.B.; Davis, I.W.; Echols, N.; Headd, J.J.; Hung L.W.; Kapral, G.J.; Grosse-Kunstleve, R.W.; McCoy, A.J.; Moriarty, N.W.; Oeffner, R.; Read, R.J.; Richardson, D.C.; Richardson, J.S.; Terwilliger, T.C.; Zwart, P.H. PHENIX: a comprehensive Python-based system for macromolecular structure solution. *Acta Crystallogr D Biol Crystallogr.* **2010**, *66*, 213-221. doi: 10.1107/S0907444909052925.

[54] Nagaraja, T.; Chen, L.; Balasubramanian, A.; Groopman, J.E.; Ghoshal, K.; Jacob, S.T.; Leask, A.; Brigstock, D.R.; Anand, A.R.; Ganju, R.K. Activation of the connective tissue growth factor (CTGF)-transforming growth factor β 1 (TGF-β 1) axis in hepatitis C virus-expressing hepatocytes. *PLoS One.* **2012**, 7:e46526. doi: 10.1371/journal.pone.0046526. Epub 2012 Oct 4. PMID: 23056332; PMCID: PMC3464290.

[55] Chen, P.P.; Li, W.J.; Wang, Y.; Zhao, S.; Li, D.Y.; Feng, L.Y.; Shi, X.L.; Koeffler, H.P.; Tong, X.J.; Xie, D. Expression of Cyr61, CTGF, and WISP-1 correlates with clinical features of lung cancer. *PLoS One.* **2007,**

2:e534. doi: 10.1371/journal.pone.0000534. PMID: 17579708; PMCID: PMC1888724.

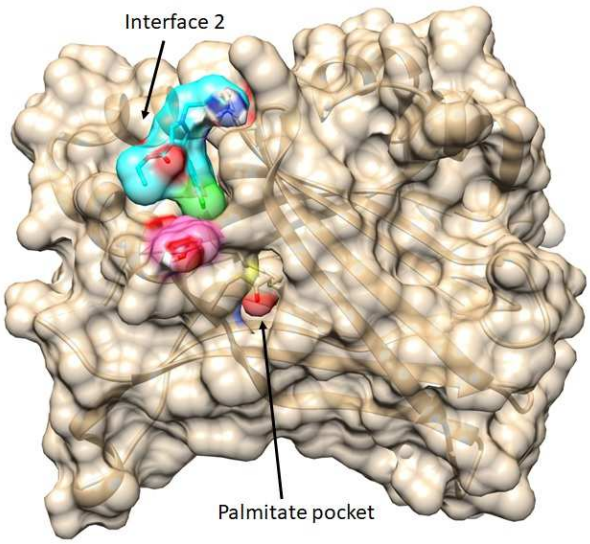

TEAD2-**6** X ray Structure

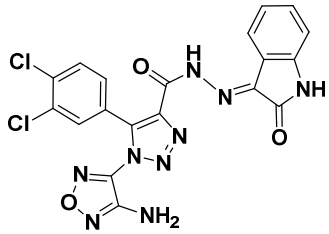

Structure-based deconstruction/optimization

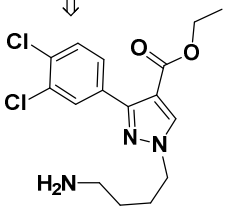

6

IC_{50} TEAD transcriptional activity = 4.5 μM
IC_{50} Breast cancer cell proliferation = 5-10 μM